RES | THE SCHOOL *for* RENEWABLE ENERGY SCIENCE

Formation of Lanthanum Zirconates in Solid Oxide Electrolysis Cells

Experimental Studies

Pedro Miguel da Costa Almeida

UNIVERSITY OF ICELAND

University of Akureyri

Formation of Lanthanum Zirconates in Solid Oxide Electrolysis Cells

Experimental Studies

Pedro Miguel da Costa Almeida

A 30 credit units Master's thesis

Supervisors:
Dr. Neal Sullivan (Project advisor)
Dr. David Dvorak (Academic advisor)
Prof. Thorsteinn I. Sigfusson (Academic advisor)

A Master's thesis done at
RES │ the School for Renewable Energy Science
in affiliation with
University of Iceland &
the University of Akureyri

Akureyri, February 2009

Formation of Lanthanum Zirconates in Solid Oxide Electrolysis Cells
Experimental Studies

A 30 credit units Master's thesis

RES │ the School for Renewable Energy Science
Solborg at Nordurslod
IS600 Akureyri, Iceland
telephone: + 354 464 0100
www.res.is

Printed in 05/05/2009
at Stell Printing in Akureyri, Iceland

ABSTRACT

Versa Power Systems solid oxide cells were tested with the objective of performing long term electrolysis testing and studying their degradation and, more specifically, the creation of insulating phases of lanthanum zirconates. Three cells were tested but only one sustained long term electrolysis testing. The other two fractured due to excessive fuel flow and lack of heating in inlet tubes. A different sealing method and bubbler were used in the third tested cell. This cell showed good initial performance with power densities around 0.32 W/cm^2 and with an ASR of 0.59 $\Omega.cm^2$ running on 175sccm H_2 / 175sccm H_20. The cell ran in electrolysis mode for 290 hours showing a steady degradation that eventually stabilized and even recovered in the last tens of hours. These are thought to be passivation and activation processes due to the silica based sealant (Hauch A. E., 2008). Scanning electron microscopy (SEM) and x-ray diffraction (XRD) measurements were performed after cell testing. They showed no significant microstructural changes and no presence of the insulating phase. A previous report on another VPS cell showed the possibility of the presence of this phase in an XRD test. Yet when a second XRD test was done these phases were not found. This might be explained if we consider that these phases form under the places where platinum paste is present, which conforms to the two different microstructural areas found in the SEM images in the previous tested cell.

PREFACE

This thesis is submitted to RES | The School for Renewable Energy Science as partial fulfillment of the requirements for the M.Sc. degree. The work presented here is the product of three months of work with solid oxide electrolysis cells (SOEC) and was mainly carried out at the Colorado Fuel Cell Center (CFCC) in the Colorado School of Mines (CSM). It was funded by RES | The School for Renewable Energy Science

This M.Sc. work is focused on the degradation of solid oxide electrolysis cells, namely, the creation of the lanthanum zirconate insulating phases, using solid oxide cells (SOC) provided by Versa Power Systems (VPS). Performance was evaluated through in situ techniques, followed by post mortem analysis to have a better understanding of the changes in the cells and formulated reasons for those changes.

These three short months in the CFCC started with an introduction to the preparation of cells for testing followed by the period in which the cells presented in this work were tested, always under the close supervision of Ph.D. candidate Darrell Eldridge and Dr. Neal Sullivan. I am very grateful for all the time and patience that Darrell had with me and also for the instructional and interesting discussions we had. He taught me how to set up the cells and how to actually test them and also what I should expect from the cell testing. I am also very grateful to Dr. Sullivan for allowing me to do my thesis in the CFCC and for all the guidance and support given during my time there.

I would also like to thank:

- Ph.D. candidate Connor Moyer for supplying the cells used for my first tests and for the tests done when developing the new sealing system;
- Everyone at the CFCC who helped me in one way or the other;
- Everyone from RES for all the hard work they put into making this school a very successful school, namely, Sigrún, Arnbjorn, Bjorn, Gudjon, David D., among others;
- My family, for all their support and for dealing with my absence while I was here;
- My friends, for the support they gave me;
- To someone special, to whom I am extremely grateful for all the time we spent together and for all the help and support she gave me during this year here in Iceland.

This year has been a great personal and professional experience and I am extremely grateful for the opportunity that was given to me last February. I met many great people and I've learned a lot during my stay here in Iceland. Thank you very much for giving me the opportunity of a life time.

Pedro Miguel da Costa Almeida, Akureyri, Iceland, 18th of February 2009

TABLE OF CONTENTS

LIST OF FIGURES

LIST OF TABLES

1 INTRODUCTION

One of the many reported problems in the use of solid oxide cells (SOC) for electrolysis is the formation of insulating phases (for example, lanthanum zirconates) during long term operation. These create ionic barriers, lower cell performance and can eventually cause cell failure due to delamination of the oxygen electrode from the electrolyte.

There are not many articles addressing this issue, and with this in mind the objective of this research is to experimentally prove that lanthanum zirconates form while operating solid oxide electrolysis cells (SOEC) during long term testing (250/300 hours). Performance and durability will be analyzed along with a literature review to provide a deeper understanding of the reasons behind the formation of these insulating phases. Post mortem analysis will also be performed on tested cells (XRD and SEM).

Chapter 2 provides background information regarding fuel cells, SOC's and lanthanum zirconates while in chapter 3 a detailed description of the test stand and experimental setup is given. Chapter 4 gives performance and degradation results obtained from tested cells as well as a post mortem analysis. A discussion of these results, based on literature review and background information, is presented in chapter 5, followed by conclusions in chapter 6.

2 BACKGROUND INFORMATION

Fuel cells are electrochemical devices which convert chemical energy directly into electrical energy without the necessity of an intermediate step. For example, in an internal combustion engine, the energy is transformed from chemical energy into work and from work to electrical energy which makes its efficiency limited by the Carnot cycle. Since fuel cells do not need this intermediate step (work) they do not have this limitation and can theoretically achieve higher efficiencies. Plus, they emit few, if any, pollutant gases like CO_2, NO_x, and SO_x, depending on the type of fuel cell used. They are similar to a battery, which can also convert directly from chemical to electrical energy, with the advantage that they can run continuously as long as fuel is provided and does not need a charging cycle before it can be used. Yet some issues are still associated with the economical side of the technology, which is still not cost competitive in most situations and some material issues also need further development, this last one being the reason for this research.

The two most known types of fuel cells are polymer electrolyte membrane cells (PEM) and solid oxide cells (SOC). The PEM cell is a low temperature cell (around 100^{o}C) which works with pure H_2. It has a fast start up time and responds well to power transients. Its down sides are that it needs careful thermal and water management, it is CO intolerant and it requires platinum as a catalyst. In this thesis, the research will be on the other type, SOC. It is a high temperature cell (between 800^{o}C and 1000^{o}C) and can work directly with some hydrocarbon fuels due to its internal reforming abilities. It has slow startup times but it is beginning to be an alternative for stationary systems, e.g. household combined heat and power systems. SOC can be used as power generators, generally known as solid oxide fuel cells (SOFC) but can also be used to produce hydrogen or syngas ($CO + H_2$) through high temperature electrolysis. When used in reverse they are known as solid oxide electrolysis cells (SOEC). The advantage of having such cells is the ability of having a single system capable of generating power when needed and producing hydrogen when a surplus of energy is available, for example, from wind turbines, solar PV systems or nuclear power plants. The produced hydrogen could later be used as fuel when operating in fuel cell mode (power generation).

This thesis will focus on a specific degradation mechanism of high temperature SOEC, which is the formation of lanthanum zirconates, and the present chapter will work as background information for the discussion of the results obtained in the research.

2.1 Solid oxide cells

As was mentioned, a fuel cell is an electrochemical device. As such it is made out of two electrodes and an electrolyte. (O'Hayre, 2006). Common materials used are:

- Electrolyte: yttria stabilized zirconia (YSZ) - ZrO_2 doped with 8%Y_2O_3 presents the highest ion conductivity (σ=0.1S/cm at 1000ºC) (Etsell, 1970), is gastight and electron insulating;
- Oxygen electrode: strontium-doped lanthanum manganite (LSM) – Stable in oxidizing atmosphere and electron conducting;
- Hydrogen electrode: nickel-YSZ cermet – electron conducting and Ni works as catalyst for H_2/H_2O reaction and fuel reforming.

Other requirements for the material choice are matching thermal expansion coefficient, sintering temperatures, durability, material costs and degree of purity (Hauch A. , 2007).

A SOC can have two possible geometries: planar or tubular. Planar cells have longer history then tubular cells yet tubular SOC are very promising since they fix the problem of sealing more efficiently (U.S. Department of Energy). More development has to be done on these in order to lower the resistance of the cell and improve its performance. In planar cells, the two most common designs are electrolyte supported cells and H_2 electrode supported cells as shown in Figure 2.1.

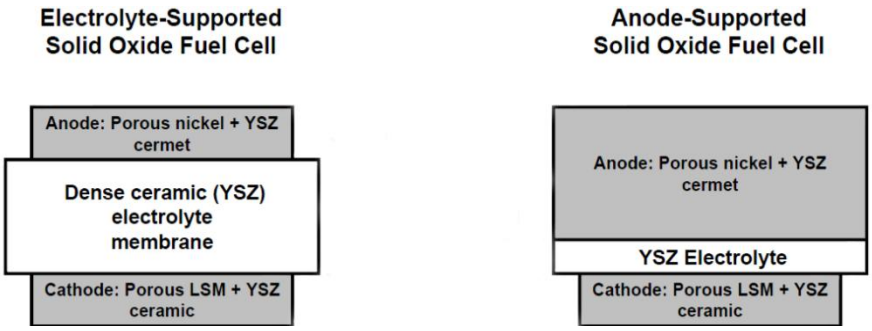

Figure 2.1 - Planar cell designs: electrolyte supported and electrode supported

The electrolyte supported cell has a 100-300 µm thick electrolyte to give it a higher mechanical strength. Electrodes are usually 10-30 µm thick. These cells are designed to work at a temperature close to 1000ºC to reduce the ionic conduction resistance since the electrolyte is so thick. To prevent issues of high temperature, like corrosion and materials cost, the H_2 electrode supported cell was developed. It has a thinner electrolyte (10-30 µm) reducing the ion conduction resistance and consequently allowing for lower temperatures (750-950ºC). Its electrodes have the same thickness, but attached to the H_2 electrode is a support layer of the same material (but more porous) with a thickness of 200-300 µm providing the structural support necessary for the cell. This is currently the most common type of SOC (Hauch A. , 2007).

2.1.1 Electrochemistry of solid oxide cells

Depending on how the cell is operated each electrode can either be the cathode or the anode. When operated as a fuel cell, the hydrogen electrode works as the anode, oxidizing the H_2 into H_2O while the oxygen acts as the cathode by reducing the O_2 into oxide ions (O^{2-}). The electrons release and travel from the anode to the cathode through a separate channel, while the ions flow across the electrolyte. This is shown in Figure 2.2.a together with the partial chemical reactions. The total reaction for SOFC when using pure hydrogen is:

$$H_2 + \frac{1}{2}O_2 \rightarrow H_2O + heat + electrical\ energy$$

When operating as a SOEC, electrical energy needs to be supplied in order for the reactions to go through and the hydrogen electrode works as cathode, reducing the H_2O into H_2, and the oxygen electrode works as anode, oxidizing the O^{2-} into O_2.

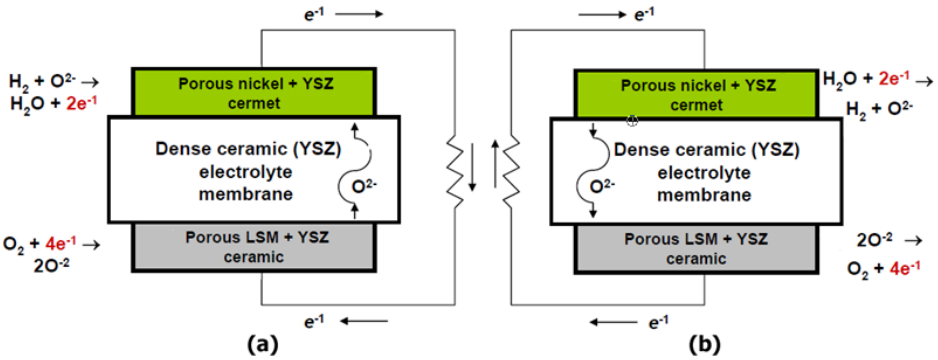

Figure 2.2 - Anode and cathode reactions for: (a) SOFC; (b) SOEC

The reactions in steam electrolysis are the reverse of those in fuel cell operation. This is shown in Figure 2.2.b. The total reaction for SOEC when using pure hydrogen is:

$$H_2O + heat + electrical\ energy \rightarrow H_2 + \frac{1}{2}O_2$$

To know the potential between the two electrodes at open circuit voltage, the Nernst equation is applied, and for SOC is slightly higher than 1 V. Yet when a load is applied the cell potential (E) will change due to polarization loses. These loses have different origins yet they are all functions of the applied current density. The polarization losses are as follows:

- η_{ohm} – this represents the ohmic overvoltage, which is the voltage expended or sacrificed in order to accomplish charge transport;
- η_{act} – this is the activation overvoltage which represents the voltage that is sacrificed to overcome the activation barrier associated with the electrochemical reaction;
- η_{conc} – this represents the concentration overvoltage which is the incremental voltage loss due to reactant depletion on the catalyst layers;

Therefore, to obtain the cell voltage for a certain set of conditions one has to subtract from the OCV all of these losses. This equation can be written as:

$$E = E_r - \eta_{ohm} - \eta_{act} - \eta_{conc}$$

where E_r is the reversible cell potential or OCV (O'Hayre, 2006). E for fuel cell operation is always smaller than E_r and for electrolysis is always larger, meaning that for electrolysis the signs of the different losses are negative. This expression is also valid for other types of fuel cell. Another important factor regarding cell performance is the availability of reactions sites. For the reaction to occur there are three necessary conditions: presence of ion conduction material (electrolyte); presence of electron conducting material (electrode); and gas presence (pores of the electrode). The area where these three conditions are satisfied is called the triple phase boundary (TPB) and is exemplified in Figure 2.3. In a SOC, a possible TPB is where the hydrogen gas turns into H^+ ions, releasing its electrons into the nickel, and meets with the incoming O^{2-} ions, forming water. So the presence of these TPB is extremely important and much research has been done in an attempt to increase them.

To measure the performance of a cell, iV curves are performed by measuring coupled pairs of cell voltage and current densities. From an iV curve, it is possible to see the effects of the different losses, even though it does not allow for quantitative assessment of most of them. It does, however, allow for the area specific resistance (ASR) to be obtained by taking the slope of the linear part of the iV curve. The ASR represents the cell ohmic resistance by unit of area. Another way to assess the cell performance is by electronic impedance spectroscopy (EIS). This allows for separate visualization of the different losses and to have a sense of which are the most significant ones (Hauch A. , 2007).

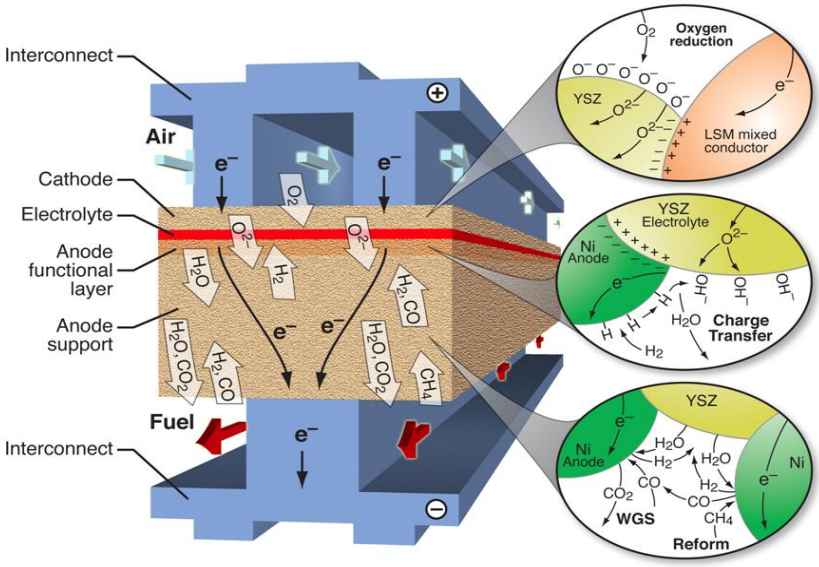

Figure 2.3 - Examples of triple phase boundaries and internal reforming reactions in SOFCs

2.1.2 SOFC development

Even though there have been many achievements in the area of SOFCs, there are still many issues that have to be addressed in order for the technology to be available commercially. These issues are more or less all connected to each other. Durability has to be improved in order to allow for the cell to last thousands of hours, and that can only be done by improvements in the cell materials, microstructure, and by having good thermal and redox cycling. Another aspect that must be looked at is cell costs, an area in which improvements should also be addressed. That includes development in cell processing techniques and improving the materials performance without raising costs (Hauch A. , 2007).

2.2 Solid oxide electrolysis cells

Recent increases in fossil fuel prices and a more aware vision of their impact in the environment has lead to an increase in the research of alternative power generation methods and in the search for an alternative fuels and energy carriers. The main issue, with these new power generation methods, like wind or solar, is that they are site-specific and intermittent, making them unreliable. Yet if the energy surplus of these sources can be stored, it will allow them to become more viable options. One effective way to store this energy surplus is by producing hydrogen through steam electrolysis. Hydrogen is currently seen as the most probable future fuel and energy carrier, yet it is produced mainly from steam reforming of natural gas, which is not renewable or clean. High temperature electrolysis (HTE) or steam

electrolysis can be a clean and effective way to produce hydrogen since it allows for its production directly from water by supplying heat and electrical energy. SOEC for HTE is more advantageous than a low temperature proton exchange membrane electrolyzers or alkaline electrolyzers since it can produce hydrogen at higher chemical reaction rate with a lower electrical energy requirement (Ni, 2008). This will be explained later on.

2.2.1 Thermodynamics and kinetics of high temperature electrolysis

As shown in Subchapter 2.1.1, the net equation for steam electrolysis using a SOEC is $H_2O + heat + electrical\ energy \rightarrow H_2 + 1/2O_2$. This is reaction is endothermic, i.e., heat is consumed, so if the temperature is increased, the reaction tends to go in the direction of the products. The total energy (ΔH) for this reaction to occur can be expressed as:

$$\Delta H = \Delta G + T\Delta S$$

where ΔG (Gibbs free energy) is the electrical energy demand and TΔS is the thermal energy demand (Ni, 2008). While ΔH remains essentially unchanged (249 kJ/mol H_2 at 900ºC) with temperature increase, the molar Gibbs free energy drops from 237 kJ/mol H_2 to 183 kJ/mol H_2 at 900ºC (Brisse, 2008). This is shown in Figure 2.4

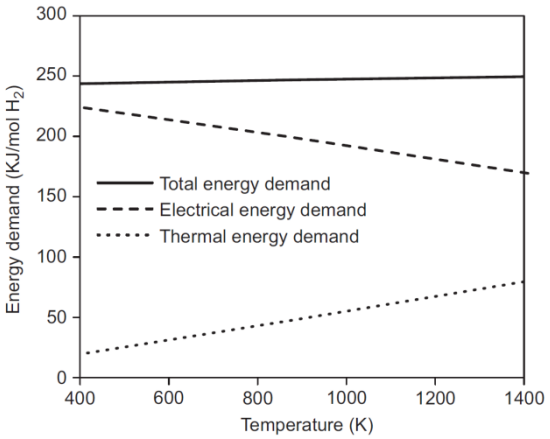

Figure 2.4 - Energy demands for steam electrolysis[1]

HTE can be performed in three different ways: endothermal, thermoneutral, and exothermal. The most favorable for low cost hydrogen production is the thermoneutral mode since it uses all the generated Joule heat from the cell for the endothermic electrolysis reaction without wasting or having the need to supply extra heat. According to Hauch (Hauch A. , 2007), for steam electrolysis, e.g. at 950ºC, the thermoneutral potential at 1 atm is:

$$E_{tn,950C} = \frac{H^{\theta}_{reac.,950C}}{nF} = 1.29\ V$$

[1] Picture taken from *Technological development of hydrogen production by solid oxide electrolyzer cell (SOEC).* **Ni, Meng et al.** 33, Hong Kong : Hydrogen Energy, 2008 (Ni, 2008)

where n is the number of transferred electrons per reaction, F is Faradays constant and $H^{\theta}_{reac.,950C}$ is the enthalpy of reaction at 950ºC. In the case of H_2O being fed in its water state, needing to be turned into steam, the thermoneutral potential is at 950ºC:

$$E_{tn,950C} = \frac{H^{\theta}_{reac.,950C} + H^{\theta}_{eva.,100C}}{nF} = 1.48\,V$$

Furthermore, higher temperatures for SOC cause a reduction on ASR which allows higher current densities and consequently a higher hydrogen production rate.

2.2.2 Possible SOEC applications

As mentioned before SOEC can, for example, be integrated in established energy generation systems. A good example of where SOECs could be implemented is the case of the Shetland Islands (Pure Project). They currently have a hybrid system that combines wind turbines with hydrogen fuel cells. During times when there is a surplus of energy, this energy is redirected to an alkaline electrolyzer, which produces hydrogen to later be used in hydrogen fuelled vehicles or other hydrogen applications as an alternative to fossil fuels. If needed, the hydrogen that is produced can also be used in a backup fuel cell generator that runs through an inverter to produce AC current for the grid. This system could be simplified by substituting the alkaline electrolyzer and back up fuel cell by a SOEC (in this case a reversible SOFC) which could run as a fuel cell or as an electrolyzer. It would reduce the area taken by the system and possibly reduce the costs of building and operating such system.

Another serious possibility is integration with nuclear power plants, since they are more efficient running at constant power (creating a greater possibility of energy surplus) and also produce high temperature waste heat. Some papers have been released regarding this combination yet no literature on actual testing of such integrated systems seems to be available (Hauch A. , 2007).

SOEC also has the potential to produce syngas if a mixture of carbon dioxide and steam is supplied. This syngas can later be used in the production of methane or methanol, or be directly used in a SOFC.

2.3 Formation of lanthanum zirconates on SOC

Perovskite-type[1] (Tejuca, 1993) strontium-doped lanthanum manganite (LSM) has been, in the last years, the most common oxygen electrode material used in SOFC. It has a high catalytic activity for oxygen reduction, is chemically compatible with yttria stabilized zirconia (YSZ) and has an acceptable thermal expansion match, three very important characteristics for a good oxygen electrode. This material, however, was originally developed for power generation; meaning that it needs to be improved in order to be used in electrolysis mode. Improvements are focused on its microstructure and interface properties to improve reversibility and durability (Guan, 2006). Generally, cells with this oxygen electrode have low durability and have a rapid decrease in performance when used in electrolysis. Other

[1] A perovskite is any material with the same type of crystal structure as calcium titanium oxide

materials for oxygen electrodes are currently being developed and have shown better results, but these materials are still in the development stage and are not a part of this study.

One of the reasons for this fast degradation is the formation of insulating phases between the oxygen electrode and the electrolyte. These phases act as a barrier to the ion conduction and greatly increase the overall cell resistance, causing low performance and durability. Lanthanum zirconates ($La_2Zr_2O_7$, abbr. LZO) are a possible insulating phase that can form under electrolysis test conditions. They are known to form during sintering of cells if the temperatures used are above 1200ºC and they have been proven to increase the resistance of cells when present (Brant, 2006). This is shown in Figure 2.5. An increase in the resistance of more than 2 orders of magnitude occurs when LZO is present.

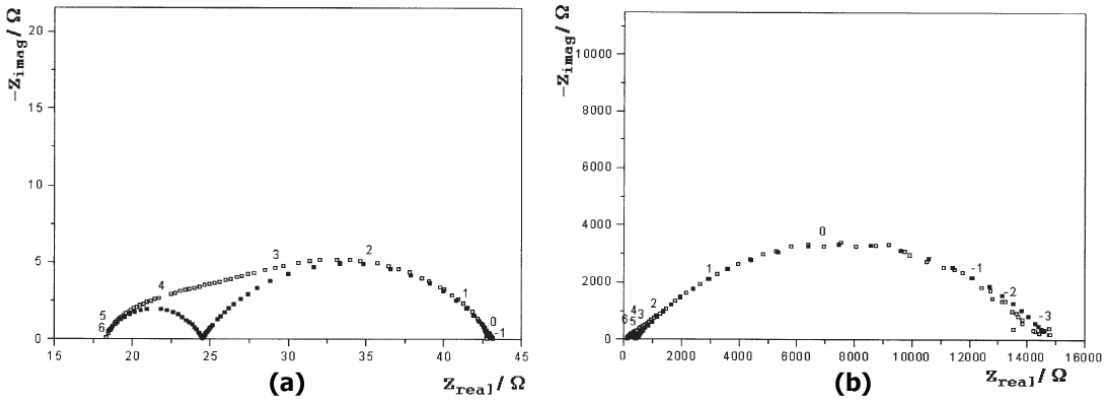

Figure 2.5 - EIS Nyquist diagrams for: a) annealing at 1100ºC; and b) annealing at 1400ºC[1]

Thus if cells are sintered at temperatures lower than 1200ºC this insulating layer should not be present. This is true if the SOC is used as a fuel cell. But if used in electrolysis mode there is a probability that this insulating layer might appear. It has been reported in some conferences that these layers form and cause severe performance degradation, causing in some cases the delamination of the oxygen electrode from the electrolyte. The reasons behind this are yet to be discovered, and this thesis aims to discover if this layer really forms when the YSZ/LSM combination is used for electrolysis purposes. There are not many articles that address this issue so some important background information about LZO needs to be known in order to prove its existence and explain its formation. According to Róg (Róg, 2002), the molar Gibbs free energy for the formation of LZO from oxides at 800ºC is 145,5 kJ/mol. This means that this amount of energy needs to be supplied for the reaction to occur. This might help to explain the creation of this insulating layer, but the most important goal of this thesis is to prove that LZO is really forming on the cell and one way to do this is by performing x-ray diffraction (XRD). Figure 2.6 shows the 2θ peaks for $La_2Zr_2O_7$ and corresponding magnitudes recorded by XRD.

[1] Picture taken from *Electrical degradation of porous and dense LSM/YSZ interface.* **Brant, M.C., Matencio, T.** 2006, Solid State Ionics (Brant, 2006)

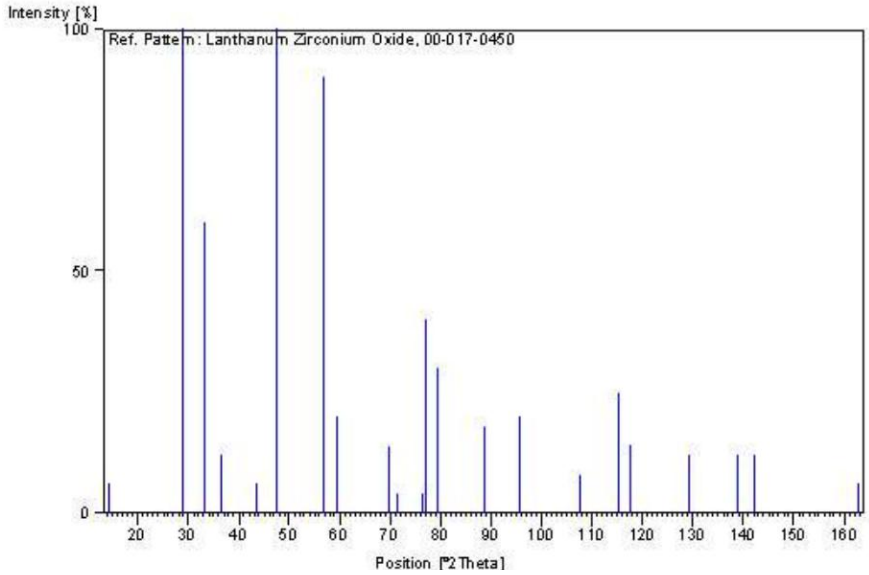

Figure 2.6 - XRD Pattern of $La_2Zr_2O_7$[1]

Chervin (Chervin, 2004) has reported the formation of these insulating phases and has attributed its cause to the use of platinum paste as current collectors for the cell, even when running in fuel cell mode. The platinum paste used contained bismuth flux compounds, to lower sintering temperatures. According to this article, the Bi^{3+} cation replaces the La^{3+}, allowing for greater La diffusion and La_2O_3 formation. This has been previously identified as a mechanism for the formation of LZO. They conclude by saying that this problem can be avoided by the use of silver pastes or platinum mesh current collectors if temperatures go above 800ºC

In 2008, Hauch (Hauch A. E., 2008) presented results on long term galvanostatic steam electrolysis of SOCs using different sealing materials. They have successfully operated a LSM/YSZ oxygen electrode cell without any oxygen electrode degradation. They found that the use of certain glass sealants promoted a passivation of the cell for the first hundreds of hours of electrolysis testing. The overall cell voltage degradation was 2%/1000h and could withstand 1300h without significant electrode microstructural changes.

[1] Taken from XRD pattern database (full report shown in Appendix B)

3 EXPERIMENTAL SETUP AND METHODOLOGY

3.1 Versa Power Systems cells

The SOCs tested in this report have been supplied by Versa Power Systems (VPS) with the intent of having them tested under electrolysis mode. Ten cells fabricated in an identical manner were provided, of which six have been tested previous to this work. A short report about the testing of those cells is provided in Appendix A. The cells are 50 mm x 50 mm with a square active area of 16 cm^2. The electrolyte is composed of 8 mol% Y_2O_3 stabilized zirconia (8 mol% YSZ). The same material is mixed with nickel oxide to form the porous hydrogen electrode and support layer. A mixture of LSM and 8 mol% YSZ is used for the porous oxygen electrode. Figure 3.1 shows a SEM image of the cell profile. Four cells not from VPS were used and tested, for training and seal testing purposes. These cells were produced by Ph.D. student Connor Moyer and their results are not part of this report since they differ from the VPS cells in geometry and production methods.

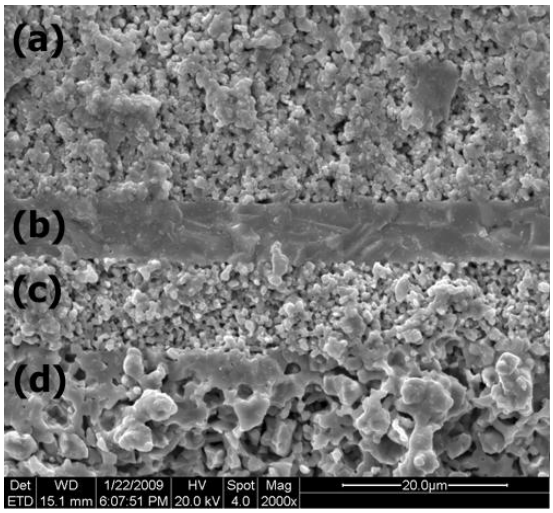

Figure 3.1 – SEM image of cell profile: a) O_2 electrode; b) electrolyte; c) H_2 electrode; d) support layer

3.2 Cell packaging

Before being able to test a cell it needs to be packaged in the gas manifolds, together with the current collectors and seals. Two different ways to package the cell were used. They basically differ in the sealant used. Failures occurred during the implementation of the first packaging method, so a second method was developed. Changing the sealing forced other changes in the packaging due to the different behaviors of the sealant materials. This is a complicated issue to deal with because the seal needs to keep the gases from both electrodes separated, not be electrically conductive to prevent shorting of the cell and at the same time be compliant enough to prevent structural stresses. This has come to be a rather complicated issue to deal with. All the seals for the experiments were hand-cut to fit the manifolds.

3.2.1 Mica seal

The first method involved the use of a compressive mica seal. This is a type of seal that has demonstrated low leak rates and good thermal cycle stability over a wide range of coefficient of thermal expansion (CTE) mismatch (Chou, 2006). Yet they are not very compliant and might create stresses if not properly centered with the cell.

The cell setup consisted of 4 mica gaskets, two small ones that fit in the gas manifolds and two bigger ones that came out of the gas manifolds, silver foil current collectors and nickel oxide paste for the hydrogen electrode side and platinum paste for the oxygen electrode side. Going from the hydrogen side to the oxygen side, the cell was setup as follows:

- Gas manifold / electric current collector – has a silver wire connected to its metallic part and the inner part of it is painted with nickel oxide paste;
- Small mica gasket – placed on top of the manifold; fits on the inside of the outer lip;
- Current collectors – Small elliptic shaped cylinders fill the whole inside of the manifold area; one of those cylinders has a longer lip that goes outside of the manifold area; this will be the voltage tap;
- Big mica gasket – sits on top of the small one and between the two comes out the voltage tap;
- Cell – painted on the hydrogen side with nickel oxide paste and on the oxygen side with platinum paste (ESL Electroscience Products), but with a grid pattern due to the paste not being porous (the Pt paste did not contain Bismuth);
- Big mica gasket
- Current collectors – the same way as those in the hydrogen side;
- Small mica gasket
- Gas manifold / electric current collectors

Figure 3.2 shows an exploded view of the cell setup without the current collectors.

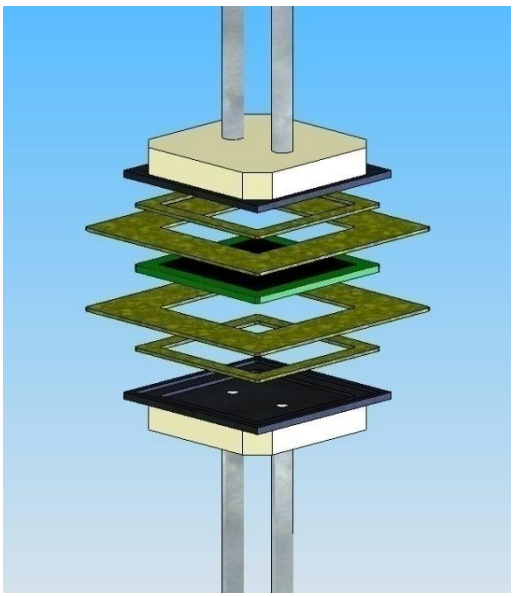

Figure 3.2 - Exploded view of the cell setup with mica gaskets

3.2.2 Alumina/silica gasket seal

In the second method, the sealant used was an alumina/silica felt (ASPS-970) produced by ZIRCAR Refractory Composites, Inc. The main advantage when compared to the mica gasket is that this material is more compliant. Even if the cell is not well centered the material can mold to the cell, preventing the creation of mechanical stresses. Yet it does not allow having a direct voltage tap as in the mica setting since the silver dissolves in it at high temperatures. So a different setting for the electrical connection of the cell had to be arranged. Thus, the final cell setup was:

- Gas manifold – in this setup a silver wire goes through the gas tubes and comes out through a 3 way Swagelok connection (shown in Figure 3.3); it is painted with nickel oxide paste.
- Alumina/silica seal – it fits inside the manifold in the same way as the small mica gasket did;
- Current collectors – "U" shaped silver mesh cylinders that are in contact with the silver wire that goes through the gas tubes;
- Cell – same as in mica gasket setup;
- Current collectors – same as those in the hydrogen side
- Alumina/silica seal
- Gas manifold

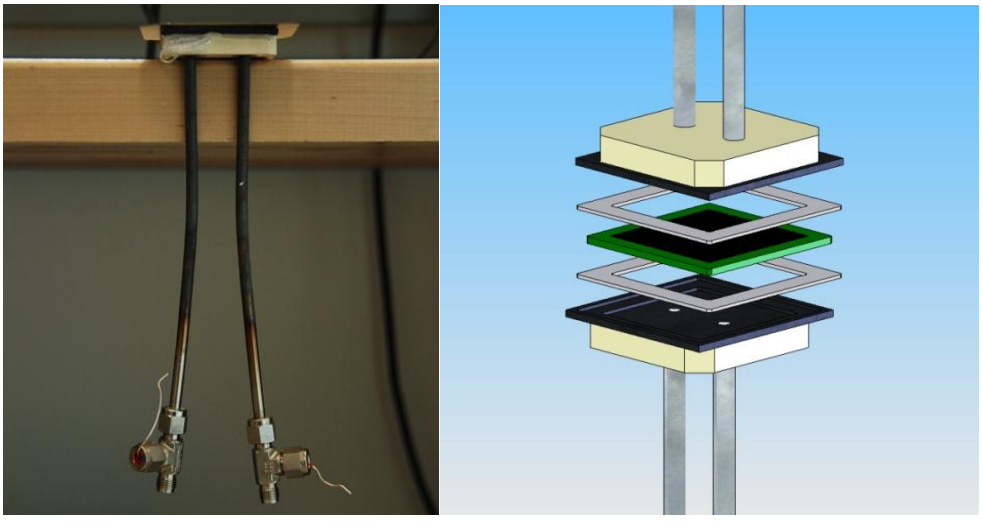

Figure 3.3 - Gas manifold with new voltage and currents taps and exploded view of cell setup with Al/Si gaskets

The reason for having a tap just for voltage is to prevent any losses due to current flow. This goes for both cell packaging methods.

3.3 Nickel oxide reduction and startup procedure

After having the cell packaged and mounted on the furnace, it is compressed with a hydraulic jack and the load applied on the cell is controlled by a spring on the top of the test stand. After being properly jacked up, the furnace is turned on and set for 800ºC at a heating rate of

2ºC/min. At the same time, air and forming gas (mixture of 97% argon and 3% hydrogen) are applied at a rate of 250 sccm (sccm – standard cubic centimeters per minute) on the oxygen and hydrogen side, respectively. Usually it is left overnight with these gas flows and, in the morning of the next day, the forming gas is turned off and the hydrogen is turned on at the same rate. The cell is left running at a constant current to help reduce the cell. In the end of that day an IV curve is taken and an EIS measurement is performed. The cell is again left over night running on 250 sccm of H_2 and air, with a constant current applied. The next day the flow on the hydrogen side is switched to 50% H_2 / 50% H_2O, usually with a total flow of 350 sccm, and another IV curve and EIS measurement are done. When finished, the cell is switched to electrolysis mode and an IV curve is run in electrolysis mode. All of these startup IV curves and EIS measurements will help to characterize the cell performance degradation after the long term testing. The cell is then left at constant current and, when finished, polarization curves are performed in the same conditions as the previous ones.

3.4 Test stand

The test stand was built by senior design team B. Curkendall, R. Donley, C. Rickers, M. Schmidt and S. Waggy in 2006-2007. It was built for SOFC testing, but it was also prepared for SOEC testing. During the period of these experiments it allowed for H_2, N_2 and forming gas to flow the hydrogen electrode, and air to flow to the oxygen electrode. Yet with minor changes it allows for the use of CH_4, CO and CO_2 on the hydrogen side and O_2 on the oxygen side. It is placed under a ventilated hood, closed with curtains to ensure good gas extraction. It is equipped with H_2 and CO sensors that control the levels of the gases being extracted to make sure none of them exceeds the safe operation limits.

In Appendix C is shown a short description of the test stand, of the electrical connections and of the flow charts. It is important to mention that two computers and two Labview programs were used. One was used to control the gas flows and the other one was connected to a Chroma DC electronic load controller, shown in Figure 3.4, which was connected to the voltage and current taps of the cell. This allowed for control of the galvanostatic load applied and to record the voltage and current read from the cell. It is from here that data is taken to create the IV curves. These programs were developed by graduate students working in the Colorado Fuel Cell Center. To prevent shorting of the cell or bad readings all the pipes were electrically isolated from the stand. The inlet pipes were also heated to prevent the steam in the hydrogen side from condensing on the way to the cell and to make sure that there was not a big temperature difference between the gases on the hydrogen and oxygen sides.

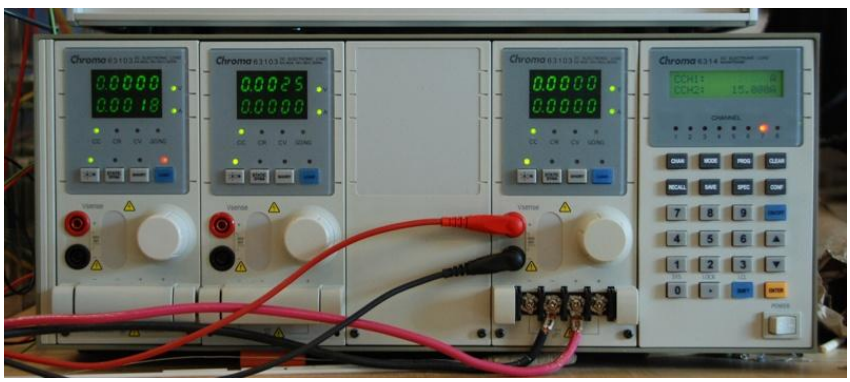

Figure 3.4 - Chroma DC electronic load controller

3.4.1 Bubbler unit / humidifier

To create a mixture of H_2 and steam, a bubbler unit was used. Hydrogen flows to the inside of the bubbler through the water, which, depending on the temperature, creates a mixture of H_2 with a certain percentage of steam. This relation is shown in Figure 3.5. Thus, maintaining a constant temperature inside is very important. This was one of the reasons why a new bubbler unit had to be made, since the old one had a heat source that was time dependant and was not insulated. This would create high instabilities in the bubbler temperature. The new one is shown in Figure 3.6. The main differences between this unit and the previous one are the heating pad around bubbler (not visible here), the insulation, the integration of a pressure transducer and PID controller. The used heating pad was an Omega SRFG-309/5-P which has 76mm width by 230mm of length with an Omega CN7833 PID controller. The pressure transducer was an Omega PX181B-030G5V with a range between 0 and 30 psi with 1 to 5 V output.

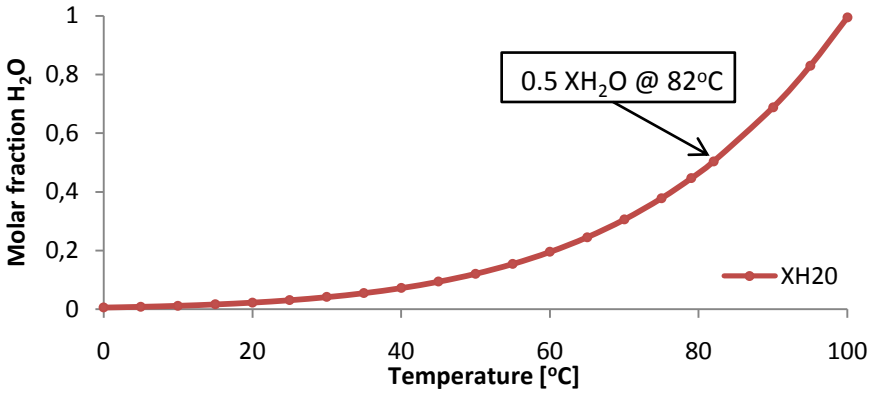

Figure 3.5 - Graphical representation of molar fraction of H_2O in function of temperature

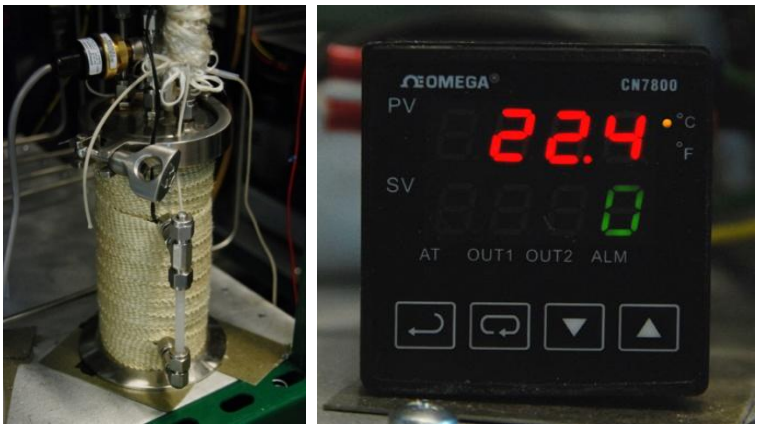

Figure 3.6 - New bubbler unit and respective PID controller

3.5 Polarization curves (IV curves)

The IV curves performed in the experiments were done galvanostatically by increments of 0.5A. To be able to compare the cell performance, three IV curves were done before and after cell testing:

- In fuel cell mode running on pure hydrogen;
- In fuel cell mode running on 50 % H_2 / 50 % H_2O;
- In electrolysis mode running on 50 % H_2 / 50 % H_2O.

Depending on the stability shown by the cells, the usual voltage limits used were 0.6 V and 1.4 V for fuel cell and electrolysis modes respectively. The voltage increments were done in the Labview program, always leaving an approx. 60 second interval between increments to allow for voltage stabilization. To create the IV curve from the data obtained from the program, the average of each step was calculated and put together in one chart.

3.6 Electrochemical impedance spectroscopy (EIS)

EIS is an in situ fuel cell characterization method that allows for analysis of the fuel cell designs and to characterize and distinguish the different fuel cell loss terms. It is performed by applying a sinusoidal voltage and measuring the respective sinusoidal current. Then, by increasing the frequency, step by step, the whole curve is obtained. The result is a curve on a Nyquist graph with units of resistance, i.e. Ohm [Ω]. An illustration of such a curve is shown in Figure 3.7. In this illustration, the different loss terms are very easily distinguishable while in reality this is a much harder job since the data points are much more dispersed and many times curves from the different losses overlap each other. It is a very useful tool for fuel cell characterization but it is time consuming and hard to apply to high power systems.

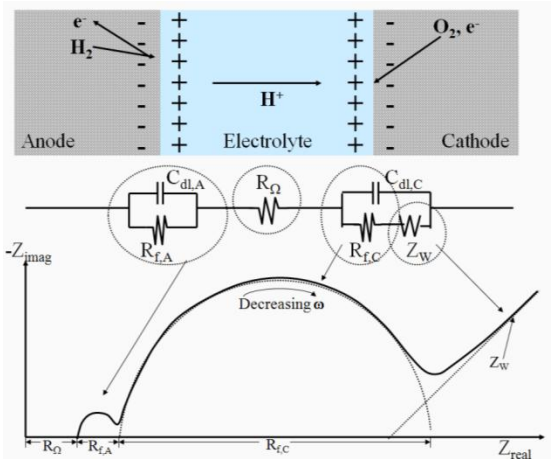

Figure 3.7 - Example of an EIS curve showing the different cell losses[1]

3.7 Post-mortem analysis

After cell testing, the manifolds are removed from the furnace and a first visual inspection of the cell is done. Using a multimeter, the cell is checked for shorts and for electrical conductivity on both electrodes. To check if cells had suffered microstructural changes a scanning electron microscopy (SEM) analysis was also performed. A FEI Quanta 600 environmental SEM was used for this effect. This machine allowed for SEM imaging and for

[1] Picture taken from O'Hayre, R. et. al. *Fuel Cell Fundamentals.* New Jersey : John Wiley & Sons, Inc, 2006 (O'Hayre, 2006)

energy dispersive spectra (EDS) even though this last one was not used. Prior to being inserted in the FEI Quanta 600, cells were gold coated to prevent charge accumulation in the electrolyte and hydrogen electrode. Images of electrodes and electrolyte surfaces and cell profile were taken at different magnitudes and some were also taken using the back scattering mode to better understand the different materials of the surfaces analyzed. The most important test, for the objectives of this thesis, was the x-ray diffraction (XRD) test, which allows for the detection of the different materials present in a sample. For this, a Philips X'Pert X-ray diffractometer with a copper tube was used. Using the copper tube allowed faster scanning times with satisfactory result accuracy. First, a fast 10º to 160º 2θ scan for peak magnitude was performed, followed by a slower more accurate scan from 10º to 90º. This smaller interval is enough to compare with the items in the database. Results from the Philips X'Pert were then put into software named X'Pert Highscore, for comparison with the available XRD database.

3.8 Conditions for testing and In-situ tests performed

Out of the four available cells for testing, unfortunately, only three of them were possible to put on the test stand due to cell testing problems and to the short time available for the experiments. Three months is very short when trying to obtain valuable experimental data. Out of the three tested cells, two used the mica gasket sealing and the old bubbler and one of them used the new Al/Si seal and the new bubbler. In all of the tested cells, IV curves and EIS measurements were performed. In the first two cells there was an attempt to run at 750ºC but due to cell failures on the third one the temperature was kept at 800ºC. Also, the flow on the third experiment was lowered due to excessive water consumption and to the possibility of having too much steam reaching the cell. Table 1 shows detailed information about the cell conditions and In-situ tests performed.

Table 1 - Cell testing conditions and In-situ tests performed

Cell	Sealant	Bubbler	IV curves					EIS
			Mode	Temperature [C]	H2 Flow [sccm]	H2O Flow [sccm]	Air Flow [sccm]	
VPS 1	Mica	Old	Fuel cell	800	100		100	
			Fuel cell	800	200		200	Same Flow Conditions
			Fuel cell	750	270		270	Same Flow Conditions
			Fuel cell	750	270		270	
			Fuel cell	750	200	200	270	
			Fuel cell	750	200	200	270	
VPS 2	Mica	Old	Fuel cell	800	270		270	Same Flow Conditions
			Fuel cell	750	270		270	Same Flow Conditions
			Fuel cell	750	200	200	270	Same Flow Conditions
VPS 3	Al/Si	New	Fuel cell	800	250		250	Same Flow Conditions
			Fuel cell	800	175	175	350	Same Flow Conditions
			Electrolysis	800	175	175	350	Same Flow Conditions
			Electrolysis	800	175	175	350	

4 RESULTS

Results will be presented separately by different In-situ and postmortem analyses performed on the cells. A comparison between different cells will be shown if it is determined to be important in the result discussion. In the subchapters for SEM and XRD, the only results presented are those of the cell tested successfully (VPS 3), of the cell tested previous to this work (also successfully) and of a reference untested cell. All results presented here were reached with the use of the facilities at the Colorado School of Mines, including the SEM pictures and XRD measurements of the old and reference cells.

4.1 Visual inspection

4.1.1 VPS cell 1

In VPS cell 1 testing, after cooling down, the furnace was opened and the first noticeable thing was that the top manifold had rotated so that it was askew, compared to the bottom one. This is shown in Figure 4.1 a). When looking at the electrode pictures, even though it is not very visible in c) (shown in red ellipse), the cell had cracked and possibly allowed oxygen to flow to the hydrogen side causing a flame. It could have caused the brighter area in Figure 4.1 b). It is also visible that the cell was properly reduced but some of the NiO paste did not get reduced.

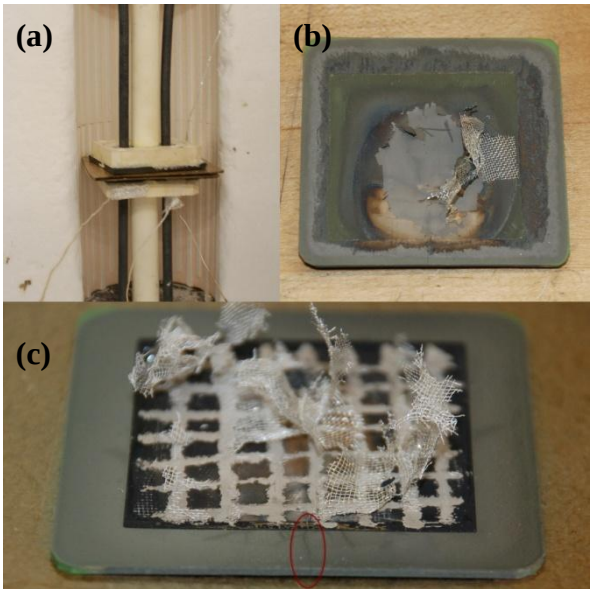

Figure 4.1 - VPS cell 1 visual inspection photographs

4.1.2 VPS cell 2

VPS cell 2, when removed from the test stand, had both manifolds aligned. No signs of rotation during testing were found. When looking at the cell it had a very obvious crack that allowed oxygen to mix with hydrogen causing a flame. This is more obvious than in VPS cell 1 due to the flow patterns imprinted in the surface of the hydrogen electrode, that come from the crack. Figure 4.2 shows proof that the cell was properly reduced.

Figure 4.2 - VPS cell 2 visual inspection photographs

4.1.3 VPS cell 3

VPS cell 3 also had the both manifolds aligned and demonstrated good adherence from the seals to the cell and also to the manifolds. The cell was properly reduced and the current collectors were glued to the cell. Yet on the hydrogen side a silver colored film was formed between the current collectors and the cell. Some current collectors stayed attached to the manifolds on both the hydrogen and oxygen sides.

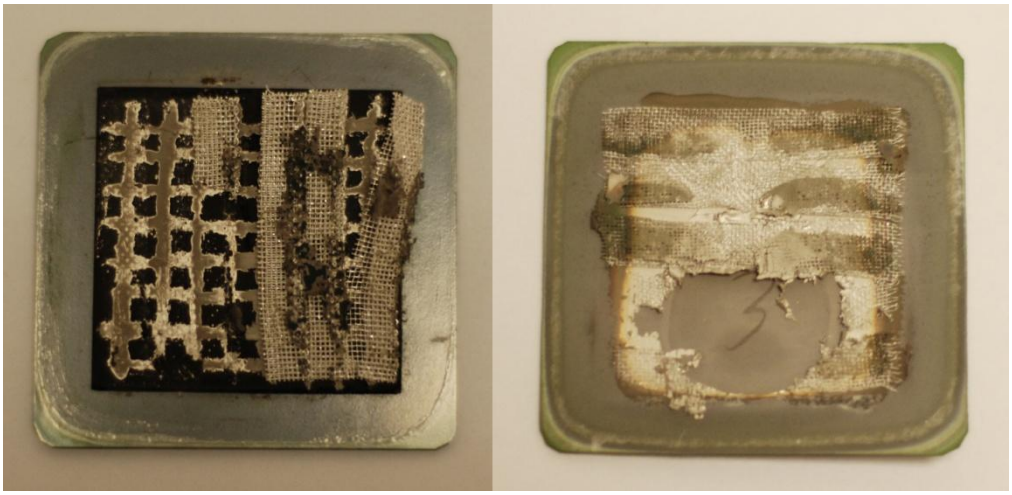

Figure 4.3 - VPS cell 3 visual inspection photographs

4.2 Polarization curves (IV curves)

4.2.1 VPS cell 1

Initially, two IV curves were taken in this cell at different flow rates. This is show in Figure 4.4. At 100 sccm H_2, OCV was 1.02 V and it is visible that the performance of the cell suffered from mass transport losses when reaching current densities close to 0.3 A/cm^2. At 200 sccm H_2 the OCV raised a little to 1.042 and any mass transport losses are no longer

visible even though peak power is reached. The maximum power at this flow rate was 0.25 W/cm^2. The ASR was similar for both flows (approximately 1.1 Ωcm^2).

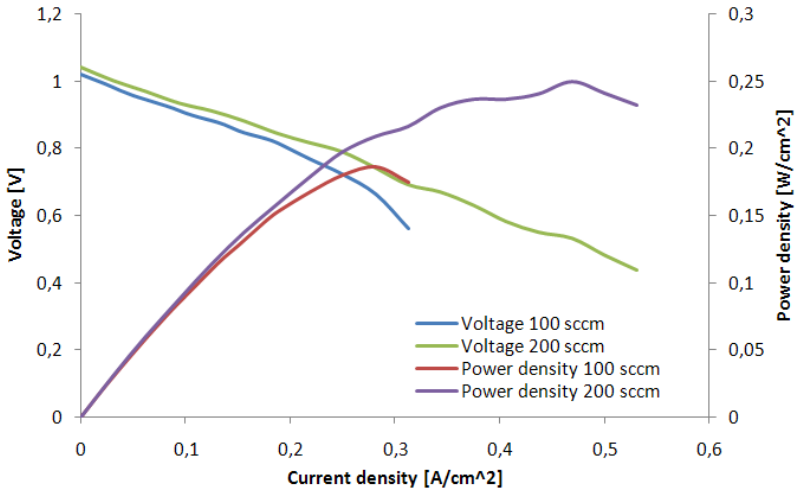

Figure 4.4 - VPS 1 initial IV curves at 800ºC - 100 / 200 sccm H_2

After these first two tests, the temperature was lowered to 750ºC and another two VI curves were taken at a flow rate of 270 sccm H_2 with approx. 12 hours between them. A comparison between one of these curves at 750ºC and the last one at 800ºC is shown in Figure 4.5. These changes generated a slightly higher OCV (approx. 1.1 V) but a lower performance from the cell, especially in terms of activation losses since the linear part of the curve remains similar to the previous results, i.e., the ASR was between 1.08 and 1.1 Ωcm^2. Afterwards, the hydrogen was forced through the bubbler unit to create a mixture of 50% steam and 50% hydrogen. The target temperature for the bubbler was 82ºC as shown in Figure 3.5, but with the old unit it was very hard to keep the temperature stable. A couple of hours later, something went wrong with the cell and its behavior became very erratic. Two IV curves were executed (one in the afternoon and the other one the next morning) that showed severe degradation of the cell. This is shown in Figure 4.6. ASR went up to 1.3 Ωcm^2 in the afternoon and to 1.5 Ωcm^2 the next morning. The maximum power density obtained in the last IV curve was 0.06 W/cm^2. Consequently the cell was shut down.

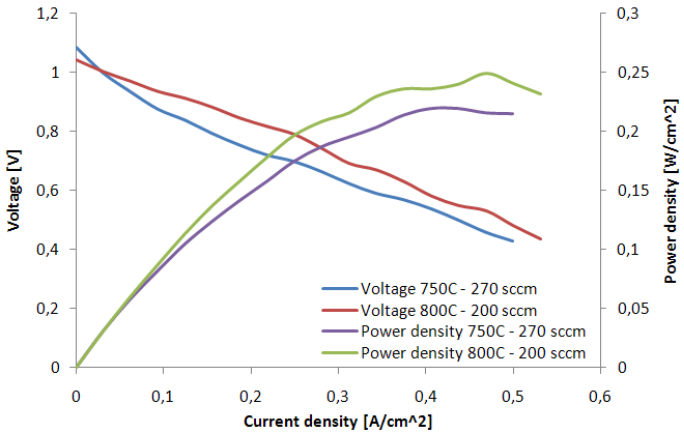

Figure 4.5 - VPS 1 IV curve comparison between 750ºC and 800ºC

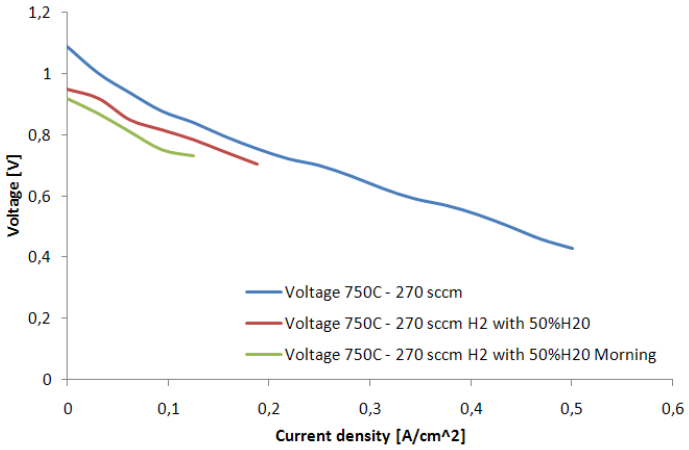

Figure 4.6 - VPS 1 IV curves after cell failure compared to curve at 750ºC

4.2.2 VPS cell 2

VPS cell 2 had a rather short run time. It had a very promising first IV curve, at 800ºC and 270 sccm H_2 with a ASR of 0.71 Ωcm^2 and maximum power density of 0.378 W/cm^2 at 0.6 V, the highest obtained by the three cells. When the temperature was lowered to 750ºC maintaining the same flow, the cell performance went down, giving an ASR of 1.04 Ωcm^2 and a maximum power density of 0.27 W/cm^2. Opposite to what had happened in previous cell the decrease in temperature caused a higher ASR, while maintaining the same curve profile at lower current densities. When switching to a mixture of 50% hydrogen / 50% steam, the cell exhibited an expected drop in OCV, yet when performing the IV curve it was not stable enough to go through the whole range of current densities as in the previous tests. Still, in the currents tested it showed a reasonable performance with an ASR of the order of 0.8 Ωcm^2. It was left running during the night at 0.25 A/cm^2 but, again, a couple of hours later the cell failed. The cell was shut down the next morning. Figure 4.7 shows the three IV curves performed on VPS cell 2.

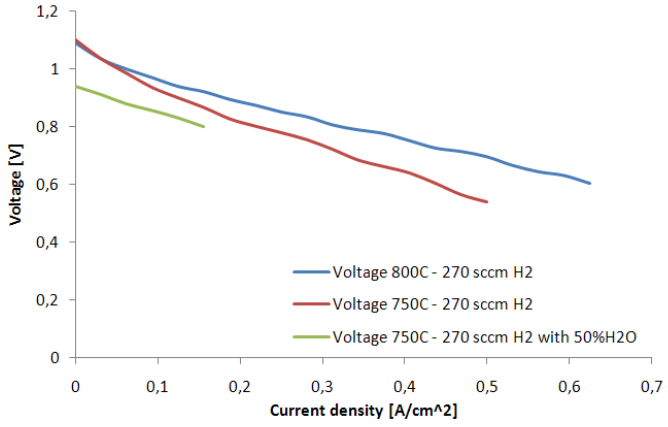

Figure 4.7 - VPS 2 IV curves

4.2.3 VPS cell 3

After testing other ways to seal the cell and installing a new bubbler unit, VPS cell 3 was put into the test stand. It was always run at 800ºC and it was the only tested cell to reach 290 hours of electrolysis testing. During this time, three events should be noted and mentioned.

Firstly, after the first 50 hours the water in the bubbler ran out and overheated the rubber tubing causing it to melt. This was fixed, the bubbler was refilled and the cell was left running on pure hydrogen for some hours in case part of the cell had reoxidized. After it came to an OCV close to what it had before, it was put back into electrolysis mode. Secondly, during the cell testing the hydrogen bottle had to be changed, which interrupted the testing for a couple of hours. Lastly, but also importantly, the air bottle ran out during electrolysis testing. It did not affect the continuity of the electrolysis testing too much since it does not need air for the reactions to occur, but when switching it back to fuel cell mode it did not allow for post testing IV curves in fuel cell mode. It was noticed that the air bottle was empty only after shutting the cell down.

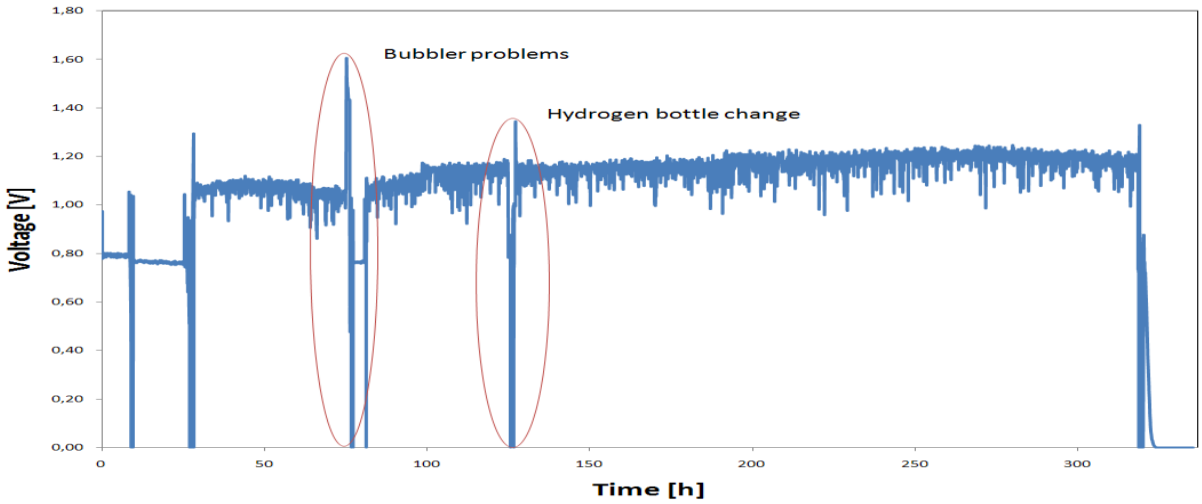

Figure 4.8 - VPS 3 long term voltage vs time

Figure 4.8 shows the time evolution of voltage during the 337 hours. Cell voltage was 1.07V in the beginning of electrolysis testing and 1.17V just before finishing. Also noticeable from this figure, apart from the erratic behavior of the data taken, is a stabilization of the cell degradation after 250 hours. Cell voltage had an increasing tendency but started leveling out and eventually even decreasing a little in the last hours of testing. During the whole testing process there was an obvious erratic behavior of cell voltage mainly because of flow problems. This will be discussed further on.

During the testing period four IV curves were taken: two in fuel cell mode and two in electrolysis mode. Unfortunately, due to the air bottle running out without being noticed, it was not possible to take any IV curves in fuel cell mode after the 300 hours of testing. The first IV curve was done at 250 sccm H_2 and showed satisfactory performance, giving a peak power of 0.325 W/cm^2 at 0,65 V and a ASR of 0.76 Ωcm^2. Afterwards, the fuel mixture was changed to 175 sccm H_2 / 175 sccm H_2O and the second IV was performed. OCV was lowered, as should be expected, but the ASR was also lowered to 0.59 Ωcm^2. The maximum power obtained was 0.317 W/cm^2, not reaching peak power, i.e., this value could be higher. Higher current densities were not tested due to instability of the flow. These two IV curves are shown in Figure 4.9.

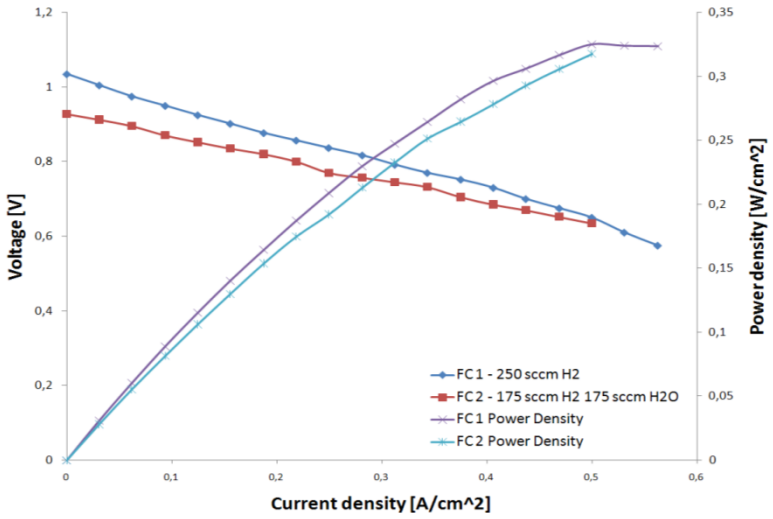

Figure 4.9 - VPS 3 Initial IV curves at pure H2 and 50% H_2/50% H_2O

After finishing the second IV the cell was switched to electrolysis mode and another IV was performed. OCV match was observed between the two IV curves (0.935 V), demonstrating continuity between fuel cell and electrolysis modes. This is shown in Figure 4.10. This first electrolysis curve showed an ASR of 0.83 Ωcm^2 and fairly decent performance. The cell was left at 0.19 A/cm^2 for a period of 290h. Afterwards another IV curve was done. Only taking into account the linear part of the curve, after long term electrolysis testing, the cell had an ASR around 0.89 Ωcm^2, which shows that the cell did not undergo much degradation. Unfortunately this last IV cannot be fully compared to the previous one since the air tank was empty and no air was flowing through the cell. Attempts to run IV curves in fuel cell mode were done but obviously they were unsuccessful. The cell was consequently shut down and left to cool down running on forming gas.

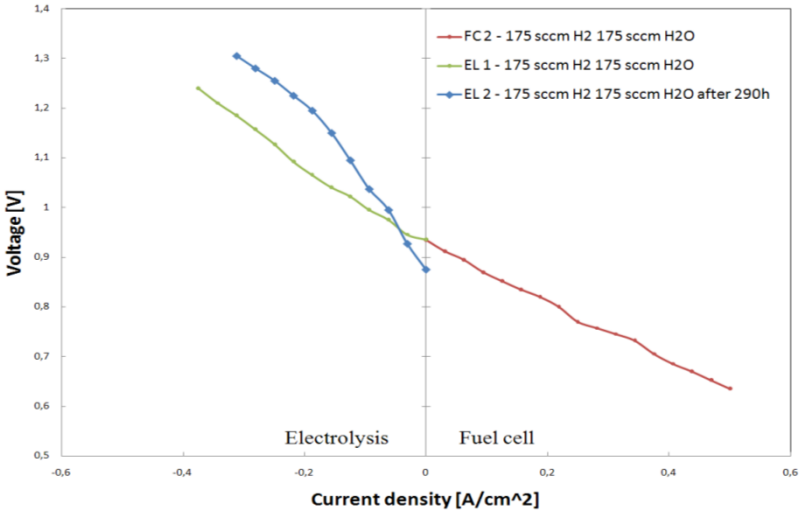

Figure 4.10 - VPS 3 fuel cell and electrolysis IV curves

4.3 Electrochemical impedance spectroscopy (EIS)

All EIS measurements were performed at low current densities, with voltages very close to OCV.

4.3.1 VPS cell 1

In VPS cell 1, two EIS curves were done: one at 800ºC and one at 750ºC. A clear increase in the electrode resistances is visible when lowering the temperature to 750ºC. In the EIS at 800ºC it can be seen that the circles for both electrode resistances are very similar. This shows that at OCV they contribute almost in the same way for the overall cell resistance. Also, the difference in electrolyte resistance in this case is very small between the two temperatures. At 750ºC only one circle is visible, most probably the one corresponding to the oxygen electrode.

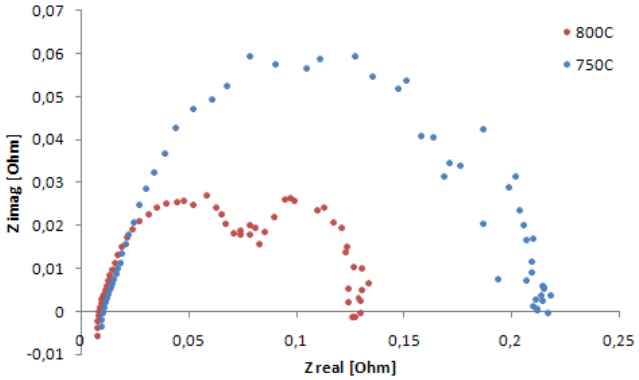

Figure 4.11 - VPS 1 EIS results for 800ºC and 750ºC

4.3.2 VPS cell 2

For VPS cell 2, three EIS curves were done: again at 800ºC, 750ºC and another one at 750ºC but running on 50% H_2 / 50% H_2O. Results for this cell are harder to interpret since the data is very widely dispersed. Still, it is possible to see a clear increase in electrolyte resistance when lowering the temperature and a decrease in the oxygen electrode resistance when the flow was switched to 50% H_2 / 50% H_2O.

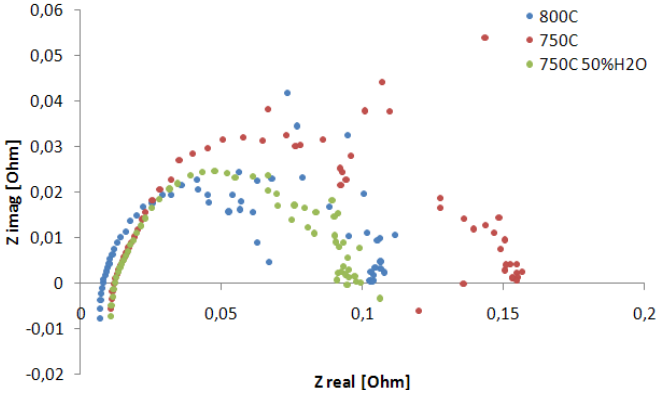

Figure 4.12 - VPS 2 EIS results for 800°C, 750°C and 750°C with 50% H_2O

4.3.3 VPS cell 3

In VPS cell 3, three EIS curves were also performed but in this case all of them at 800 ºC. The first one was done with pure H_2 followed by another with a 50/50 mixture of hydrogen and steam. After 290h of cell testing another EIS was performed at 50% H_2 / 50% H_2O. All three of the tests showed very similar electrolyte resistance. Between pure H2 and 50/50 mixture a decrease in electrode resistance was detected once again. After 290h, the cell had an increased electrode resistance and showed evidence of mass transport losses. Again, this last EIS can show a different behavior from what the cell should present due to the absence of air in the oxygen electrode.

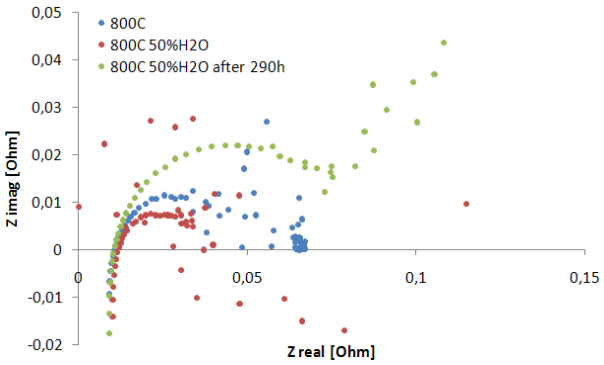

Figure 4.13 - VPS 3 EIS results for 800°C, 800°C with 50% H2O and after electrolysis testing

4.4 Scanning electron microscopy

SEM images at larger magnification for these cells are found in Appendix D.

4.4.1 Reference cell

This cell was used as a reference cell since it was put to the test stand, reduced and not tested since it did not present good initial performance. This weak initial performance was due to cell packaging problems and not due cell problems. This is described in Appendix A (it was the third cell tested in that report). It is visible in picture (a) of Figure 4.14 the four layers that form the cell (from top to bottom): oxygen electrode; electrolyte; hydrogen electrode; and support layer. The other two images, (b) and (c), show the oxygen electrode and hydrogen electrode respectively.

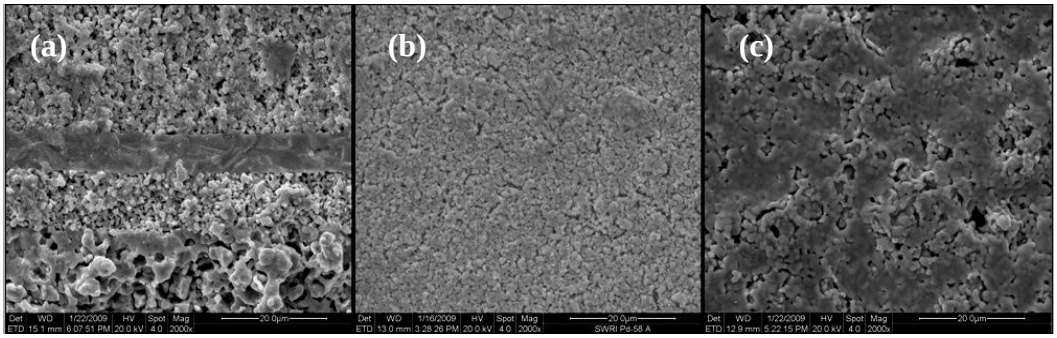

Figure 4.14 - SEM images of reference cell: a) profile, b) oxygen electrode and c) hydrogen electrode

4.4.2 Old cell

This cell was tested in the CFCC previous to this work. It was run for 310h hours at 0.25 A/cm^2. It had a much more severe degradation than VPS cell 3. Its voltage went from 1.24V at four hours of testing to 1.47 V after 310 hours. After disassembly, the O_2 electrode delaminated from the electrolyte and was found to be well adhered to the silver current collectors. A visual inspection showed no irregularities in the H_2 electrode. The testing and results of this cell are shown in Appendix A.

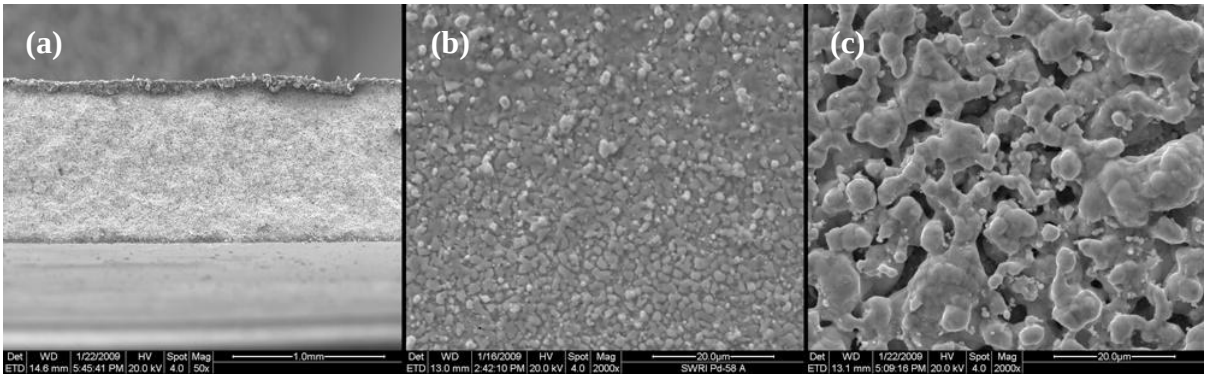

Figure 4.15 - SEM images of old cell: a) profile, b) oxygen electrode and c) hydrogen electrode

SEM pictures of this cell were taken and are shown in Figure 4.15 and Figure 4.16. Looking at picture a) from Figure 4.15 it is clear that no oxygen electrode is present. When looking at the surface, where this electrode should be, a completely different microstructure from that of the reference cell is found. Also, the microstructure of the delaminated electrode (Figure 4.16) is different from the reference cell. What is curious about both of these surfaces is that both of them have two different microstructures in them: where there was platinum paste on top (area inside red square (c)); and where there was no platinum paste (b). Where there was platinum paste the surface is smoother, while in the other area a much rougher microstructure is present, showing what looked like crystalline spikes. Finally, the microstructure of the H_2 electrode (Figure 4.15 (c)) had much bigger grains than the reference cell.

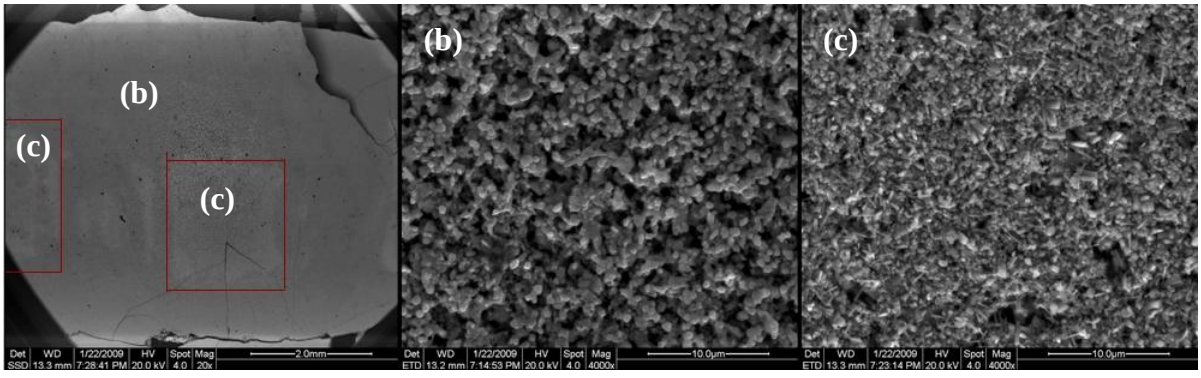

Figure 4.16 - SEM images of the two zones present in the delaminated electrode

4.4.3 VPS cell 3

This cell, as stated previously, was run at a current of 0.189 A/cm^2 in electrolysis mode for a period of 290h, during which time no delamination occurred. Looking at the SEM pictures of the profile and electrode surfaces these are very similar to the reference cell. Only the H_2 electrode shows a slightly higher concentration of areas without grains but this could be observed-area dependant.

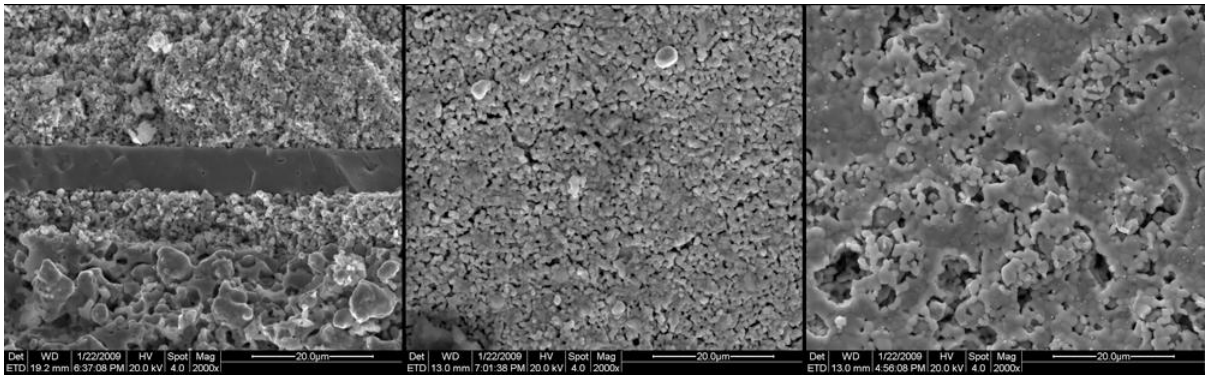

Figure 4.17 - SEM images of VPS cell 3: profile, oxygen electrode and hydrogen electrode

4.5 X-ray diffraction (XRD)

In all XRD graphs three lines have been placed where the peaks for LZO should be present. The oxygen electrode or interface between this and the electrolyte were the targets of the XRD measurements.

4.5.1 Old cell

Both in the XRD results for the cell and for the delaminated electrode no peaks were found that matched the peaks of LZO. This is shown in Figure 4.18 and Figure 4.19.

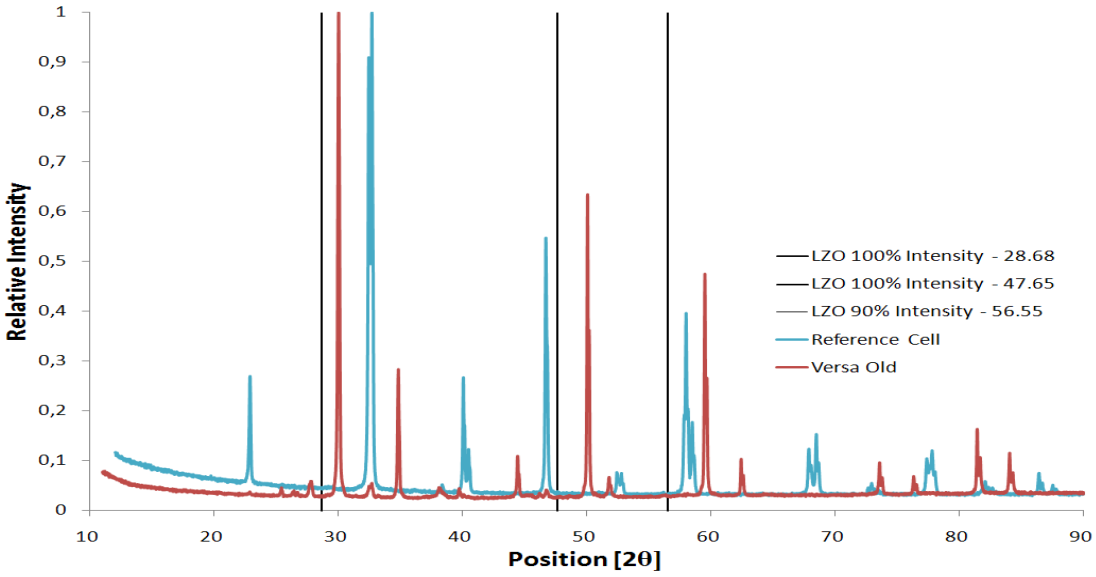

Figure 4.18 - XRD of old VPS cell

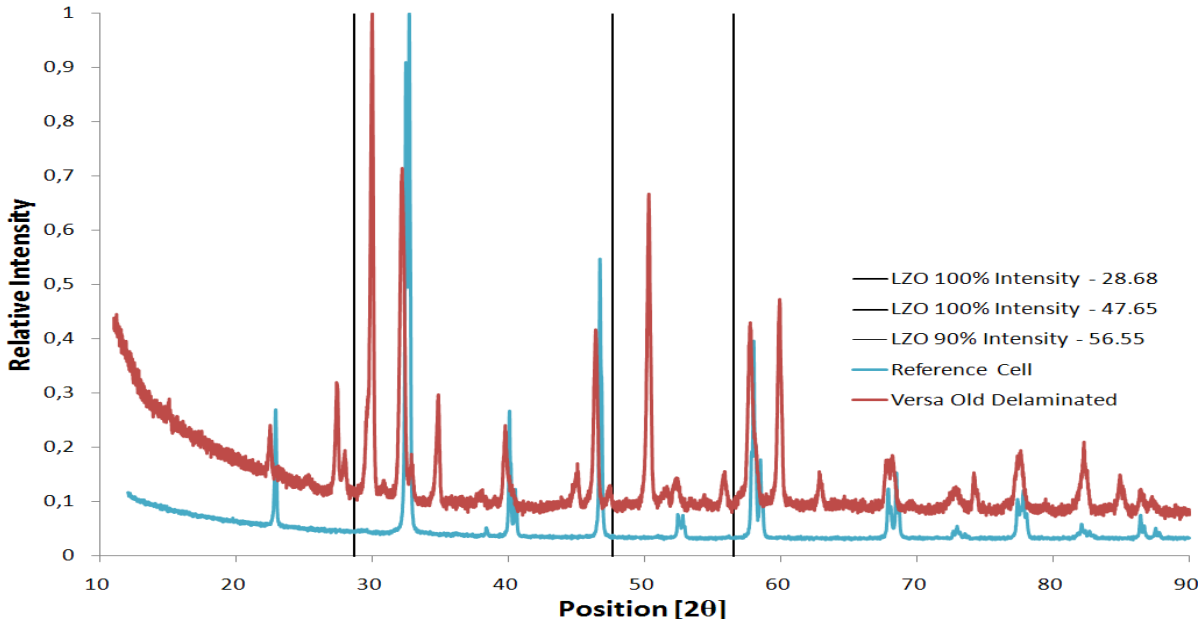

Figure 4.19 - XRD of old VPS cell delaminated electrode

4.5.2 VPS cell 3

No evidence of LZO is found through XRD measurement here. The appearance of new peaks is obvious but no set of peaks that match the ones from LZO. This is shown in Figure 4.20.

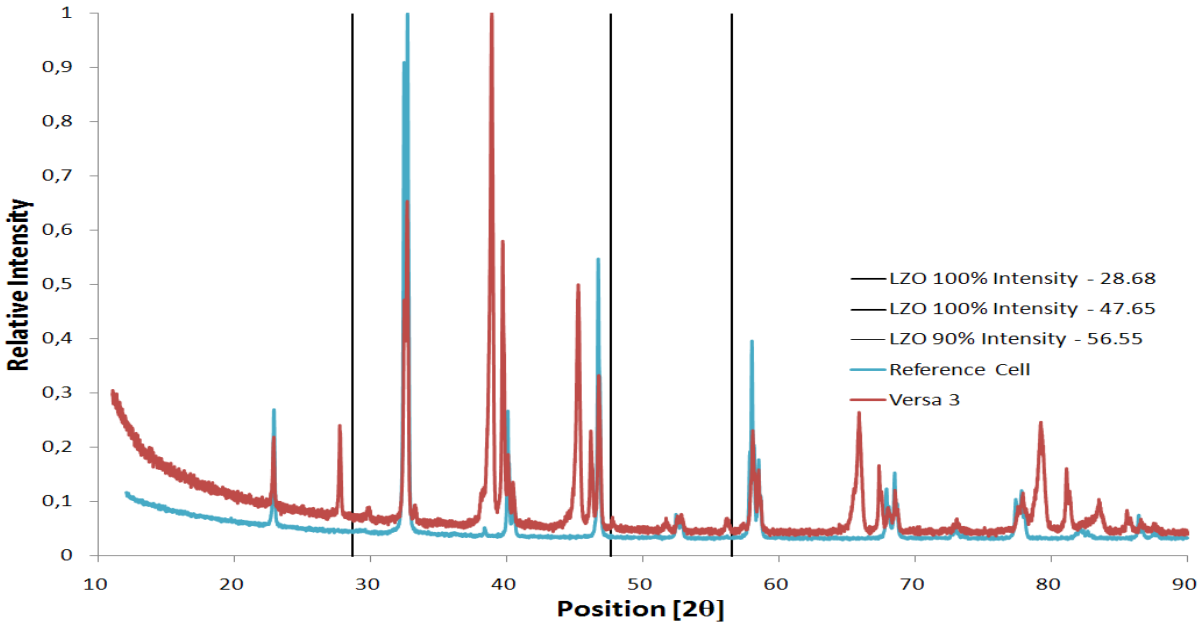

Figure 4.20 - XRD of VPS cell 3

5 DISCUSSION OF RESULTS

Starting with the cell packaging method, between the two methods, the second one proved to be more effective. The mica gaskets turned out to not be very compliant and might have caused stresses on the cell since the small gasket could slide on the big one and throw the whole setup out of alignment. This might have been one of the causes of the VPS cell 1 and 2 failures. Having the direct voltage tap from the cell ensured a correct reading of the cell voltage but at the same time this thin silver mesh could break easily. The Al/Si setup seemed to have solved the problem of the mechanical stresses but not enough tests were made to create an established cell setup. The reason for the use of "U" shaped cylinders was just ease of manufacturing them while assuring a good area of contact.

Regarding the test stand some points should be mentioned. Starting with the old bubbler, as was mentioned earlier it could not maintain a constant inside temperature. The old heat strip was based on the percentage of working time and many times the temperature dropped or raised severely due to being in an off or on period. Plus it did not have any insulation, which made it more difficult to maintain a certain temperature. So a new bubbler unit was made, with a heat strip and thermocouple connected to a PID controller, allowing a stable temperature to be achieved. This new bubbler assembly included a Swagelok "T" connection for easier refill, i.e., without the need for opening the whole unit. What may have helped to cause the failure of the first two cells was the fact that strips that heat the pipes were not on. They were thought to turn on when the bubbler unit turned on but this was incorrect. This possibly allowed for water to condensate in the pipes. Besides that, in the first two cells, an excessive flow was being inserted into the cell causing stresses in the cell and possibly helping to crack it. Also, in the last performed cell tests (including non-VPS cells) the fuel flow exhibited an erratic behavior. This caused big variations in the cell voltage recorded. The Swagelok connections were checked for leaks and no leak was found. The reason for this erratic flow was not found but it was suspected that one of the mass flow controllers was not working properly. Also, the fact that the silver wires for voltage and current taps were going inside the piping might have helped this erratic behavior. Finally, regarding the test stand, it would be better if both flow control and load control were integrated in the same Labview program in the same computer. This would allow for easier control of the testing conditions and facilitate the data acquisition of flow, electric and temperature variables.

Before talking about the results of each cell, I would like to mention that EIS measurements presented in this report will not have a lot of attention in this discussion since they were done at OCV conditions. They were not done at the operating current densities and do not represent the conditions at those current densities. This was due to an improper background search on EIS measurements and to the short time available.

Concerning the three tested cells it was evident that the first two cells had a very premature end of life. The first part of this discussion will focus on establishing a reason for these failures. This will be followed by a discussion of the results from the third cell and a final discussion concerning the insulating phase that was looked for in this thesis.

Starting with VPS cell 1, unfortunately there were many things that might have caused this cell to fail and it will be difficult to reach a conclusion regarding this. Firstly, right after the furnace was opened the top manifold clearly was rotated compared to the bottom. The most probable cause for this rotation is the pipes that were connected to the manifold. If the pipes, after installation, are not in a resting position they can create forces in the manifold causing it to move. What also helped was the fact that the two mica gaskets can easily slide on one

another. Two other things mentioned in this discussion could have also been causes for the failure: the non heating of the inlet pipes and the excessive flow put on the hydrogen side. This is also true for VPS cell 2. When looking at the results from these two cells, both of them exhibited good performance in the first polarization curves running on pure hydrogen. They presented good stable voltage and acceptable power densities and ASR's. Only when switching to a mixture of 50% H_2 / 50% H_2O did the cells start showing signs of instability and eventually failure. Also important to mention is that both cracks (in VPS cell 1 and 2) were on the side of the fuel inlet pipe right where the gases are coming to the inside of the cell.

When the temperature was lowered in cell 1, ASR remained similar to the previous polarization curves, when the expectation was that it would increase. The fact that the cell was left at 0,7 V overnight between the tests at 800ºC and 75OºC might explain this since more time was given for the cell to reduce properly. In cell 2, when the temperature was lowered the ASR increased as would be expected.

VPS cell 3 was the only cell tested successfully in electrolysis for 300h during this three month period. Many things were changed and improved for the testing of this cell. First of all the new bubbler system was a great improvement in the test stand. The PID controller allowed for the temperature of the bubbler to remain much more constant and much closer to what was desired. Also the new sealing material proved to be effective. During its use, good OCVs were obtained and they endured the whole testing cycle without breaking or being destroyed. They revealed good adherence to the surfaces of the cell, which helps in the sealing process of the cell.

During the whole testing period the cell showed a muted degradation (around. 9.3% / 300h) and seemed to have stabilized or even recovered from this degradation. This was an unexpected phenomena but it was also reported to happen in the journal article by Hauch. A. (Hauch A. E., 2008). According to this report, their tested SOEC usually suffer from an initial passivation[1] effect in the first hundreds of hours, followed by an activation[2] effect. They also report that this is due to the presence of silica in the sealing material which fits with the sealing used in this cell. So it is thought that this stabilization and recovery might be associated to the type of sealant used.

One of the problems encountered during this cell testing was the depletion of the air bottle. This did not cause any apparent problems for the cell when running in electrolysis mode. Yet the fact that the there was not air flow through the oxygen electrode might have created an increase in the resistance related to this electrode since nothing was flushing out the produced oxygen. Of course in fuel cell mode, the cell did not work properly. I wasn't even able to maintain a constant OCV. So it means that the registered OCV in the last electrolysis polarization curve could have possibly been higher.

Even though the cell performed well, when it was removed from the test stand, it had a strange silver colored film between the hydrogen electrode and the silver mesh. The reason for the creation of this film is to this moment unknown but it is possible that it might have been created during the time when the bubbler had problems. It allowed for air to go inside the fuel mixture and might have caused a flame close to the electrode.

Regarding the SEM pictures, it is evident that the old VPS cell suffered a huge degradation. The hydrogen electrode had much larger grains, reducing the TPB area available and consequently reducing its performance. Even more evident is the delaminated electrode that

[1] Passivation is a reversible or partly reversible loss in performance from the cell.
[2] Activation is the recovery of cell performance.

perfectly detached itself from the electrolyte. When analyzed it displayed different microstructural areas, as was said before. The reason for this is surely the presence or absence of platinum paste, but it still does not explain why one surface has a rough microstructure and the other one does not. This might have occurred due to preferential electron flow through the areas where there was platinum paste since it had better electrical connection with the current collectors. When looking at SEM pictures of the VPS cell 3, the microstructure showed almost no changes when compared to the reference cell. This goes well with the data from the electrical tests performed in the cell.

When XRD was done in the old cell in the summer of 2008, before these experiments, the presence of lanthanum zirconates in the cell was suspected. XRD, performed by me, showed no evidence of this compound in the cell neither on the cell nor on the delaminated electrode. No signs of this compound were found in VPS cell 3 either.

6 CONCLUSION

Regarding cells 1 and 2, the evidence for their failure points to the fact that the heating of the pipes was not turned on and that excessive flow was being supplied to them. It is also possible to conclude that the new cell packaging method was a successful alternative to the mica gasket. Yet I also consider the mica gasket a good way to package the cells as long as the proper care is taken to keep the different gaskets and cell centered. Looking at the SEM of the delaminated electrode from the old cell, to prevent the presence of two different microstructures in the electrode the platinum paste should be porous and be spread through the whole electrode area.

In summary, this was not a successful experiment in the sense that what was looked for was not found. The presence of lanthanum zirconates was reported in the previous report from the VPS cells, which leads to the possibility that these insulating phases formed locally and under the areas where there was platinum paste. This might explain why it was found in one XRD measurement and not on the other. As a future experiment, small pieces of the areas that had platinum or not could be examined separately to confirm this.

Many problems were encountered during the testing of the cells and my personal inexperience helped in some of the bad results from these experiments. But if seen from another point of view, it was successful since in three months a new packaging method was developed, one VPS cell was tested for 300h and could have operated longer if more time was available. For me personally, I developed an important skill set: I learned a lot about the testing of SOC, both in fuel cell mode and electrolysis mode.

REFERENCES

Brant, M. M. (2006). Electrical degradation of porous and dense LSM/YSZ interface. *Solid State Ionics* .

Brisse, A. S. (2008). High Temperature Water Electrolysis in Solid Oxide Cells. *International Journal of Hydrogen Energy* .

Chervin, C. G. (2004). Chemical degradation of LSM/YSZ composite cathodes in the presence of current collector pastes. *Solid State Ionics* .

Chou, Y. S. (2006). Compressive Mica Seals for Solid Oxide Fuel Cells. *Journal of Materials Engineering and Performance* .

ESL Electroscience Products. (n.d.). Retrieved February 18, 2009, from http://www.electroscience.com/pdf/5542.pdf

Etsell, T. a. (1970). Chemical Reviews. *70*, 339.

Guan, J. M. (2006). *High performance flexible reversible solid oxide fuel cell.* Torrance, CA: GE Global Research Center.

Hauch, A. E. (2008). Solid Oxide Electrolysis Cells: Microstructure and Degradation of the Ni/Yttria-Stabilized Zirconia Electrode. *Journal of The Electrochemical Society* .

Hauch, A. (2007). *Solid oxide electrolysis cells - Performance and durability.* Roskilde: Riso National Laboratory, Technical University of Denmark.

Mitterdorfer, A. a. (1998). LaZrO formation and oxygen reduction kinetics of the LSM/YSZ system. *Solid State Ionics* .

Ni, M. L. (2008). Technological development of hydrogen production by solid oxide electrolyzer cell (SOEC). (33).

O'Hayre, R. e. (2006). *Fuel Cell Fundamentals.* New Jersey: John Wiley & Sons, Inc.

Pure Project. (n.d.). Retrieved January 14, 2009, from http://www.pure.shetland.co.uk/html/pure_project1.html

Róg, G. K.-R. (2002). Determination of the standard molar Gibbs energy of formation of lanthanum zirconate by a galvanic cell involving lanthanum beta-alumina electrolyte. (34).

Tejuca, L. G. (1993). *Properties and applications of perovskite-type oxides.* New York: Dekker.

U.S. Department of Energy. (n.d.). Retrieved February 12, 2009, from http://www.fossil.energy.gov/programs/powersystems/fuelcells/fuelcells_solidoxide.html

APPENDIX A

This is part of a report submitted by the Colorado School of Mines on the 3rd of June of 2008 to Versa Power Systems.

Task 2: Electrolysis Testing

In the second task of this program, CSM has evaluated the electrochemical performance of solid-oxide electrolysis cells (SOECs) fabricated by Versa Power Systems. VPS provided CSM with ten SOECs for this evaluation. All cells were fabricated in an identical manner. All cells measured 50mm x 50mm, with an active area of 40mm x 40mm (16cm^2).

CSM is evaluating the electrochemical performance of these cells in the test stand currently available at the Colorado Fuel Cell Center. The test stand was initially modified to properly package the VPS cell. Unfortunately, the first two cells were broken during installation and startup. The third cell was successfully installed, and brought through startup procedures, but yielded lower-than-expected power density during electrochemical testing in fuel-cell mode (maximum power density of 0.15 W/ cm^2 under flooded hydrogen conditions at 800°C). Because of this low power density, the cell was removed from the test stand for inspection. Photographs of the cell are shown in Figure 3.

These images indicate no cracking of the membrane-electrode assembly, adequate reduction of the active area on the fuel side of the cell, and strong adherence between the electrodes and the silver-mesh current collectors. Two of the current collectors on the fuel-side electrode remained attached to the metallic interconnect in which the cell was packaged. While this visual inspection was encouraging, the density of current collectors and method of application for the platinum contact paste could be improved, and may have played a role in the low power density observed in fuel-cell mode. CSM addressed this shortcoming in subsequent tests.

After seeing these images, engineers at VPS requested a change in sealing method. CSM had been experimenting with several materials; the best success was found to be mica gasket material, with the cell placed in compression to promote sealing. This technique was used with VPS Cell 3 shown in Figure 3. In packaging VPS Cell 4 for electrochemical testing, CSM employed a porous zirconia felt for sealing the cell within the test fixture. Unfortunately, this change did not produce the desired result, as Cell 4 was cracked during testing, yielding no reliable electrochemical-performance data.

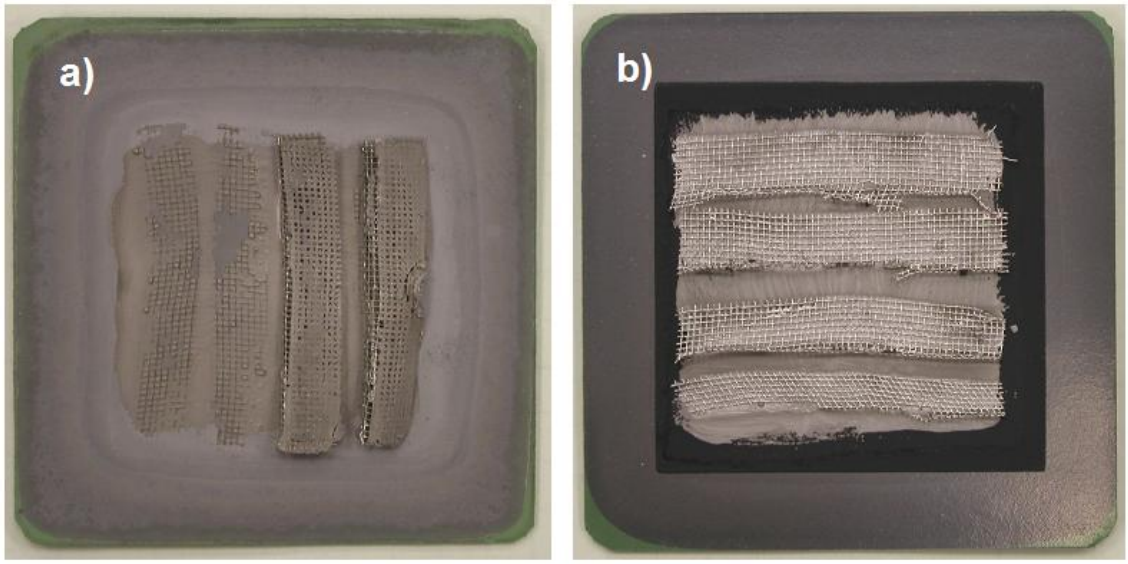

Figure 3: Images of VPS Cell 3 after ~ 48 hours of electrochemical testing in fuel-cell mode: a) fuel-side electrode; b) air-side electrode.

VPS Cell 5 was subsequently loaded into the test fixture using the mica-gasket sealing approach that was employed in packaging Cell 3. Cell 5 was brought to operating temperature of 800°C and reduced under forming gas (3.5% H_2, balance argon) for a period of 24 hours. The cell was then exposed to hydrogen fuel and air oxidizer, achieving an open-circuit voltage of 1.110 V. The cell was then tested in fuel-cell mode, achieving 0.39 W/cm^2 at 0.7 V under pure hydrogen fuel flowing at 350 sccm at 800°C.

The fuel stream was then switched to a composition that was amenable to electrolysis-mode testing, utilizing a composition of 250 sccm forming gas, 125 sccm of hydrogen, passed through a bubbler unit containing deionized water held at 60°C. The cell was driven at a constant current of 4 amps (0.25 A / cm^2), and the cell voltage was measured over 310 hours of continuous operation in electrolysis mode. The change in cell voltage over time is shown in Figure 4. The cell potential was found to increase fairly linearly with time, rising from a value of 1.24 V at four hours of testing to 1.47 V after 310 hours.

CSM ran polarization curves spanning fuel-cell and electrolysis-mode conditions before and after long-term testing; results are shown in Figure 5a. Cell performance was found to decline significantly. Electrochemical impedance spectroscopy was also performed at open-circuit conditions, with results shown in Fig .5b; a large increase in the overpotential of the air-side electrode is observed after long-term testing.

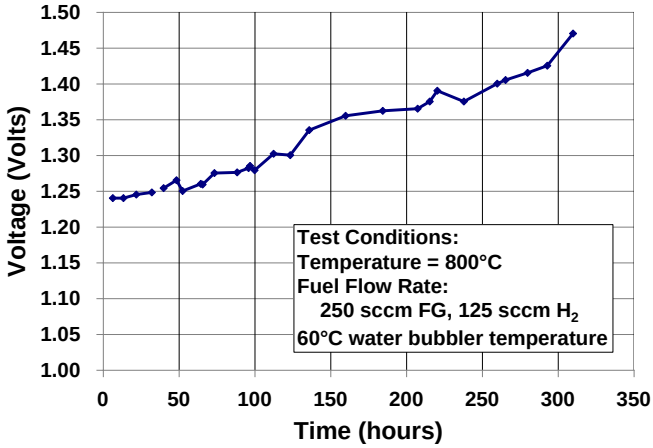

Figure 4: Cell voltage over time during testing in electrolysis mode at 0.25 A / cm^2

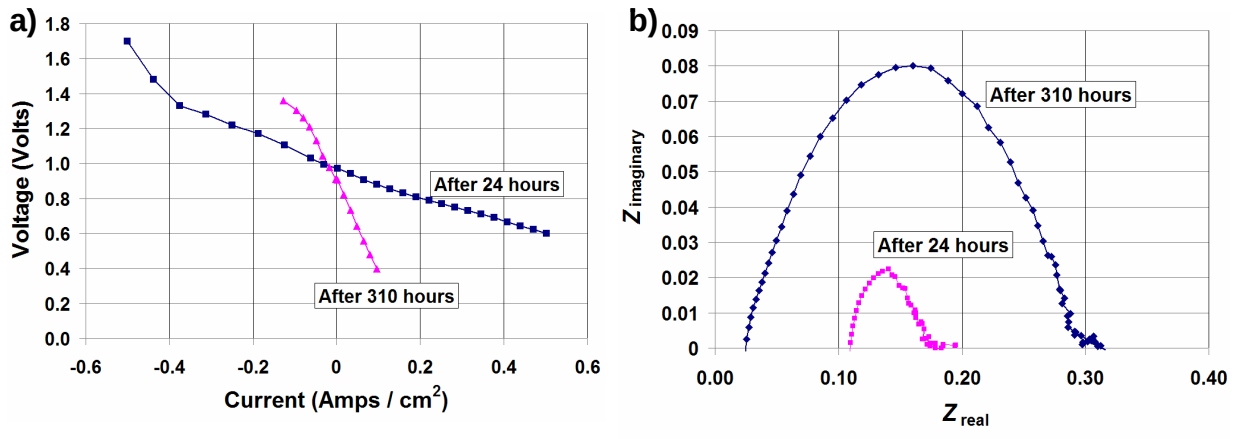

Figure 5: Comparison of cell performance before and after electrolysis-mode testing: a) polarization curve; b) electrochemical impedance spectroscopy.

To investigate the source(s) of this performance degradation, the cell was removed from the test stand for analysis. Photographs of the cell after disassembly from the test stand are

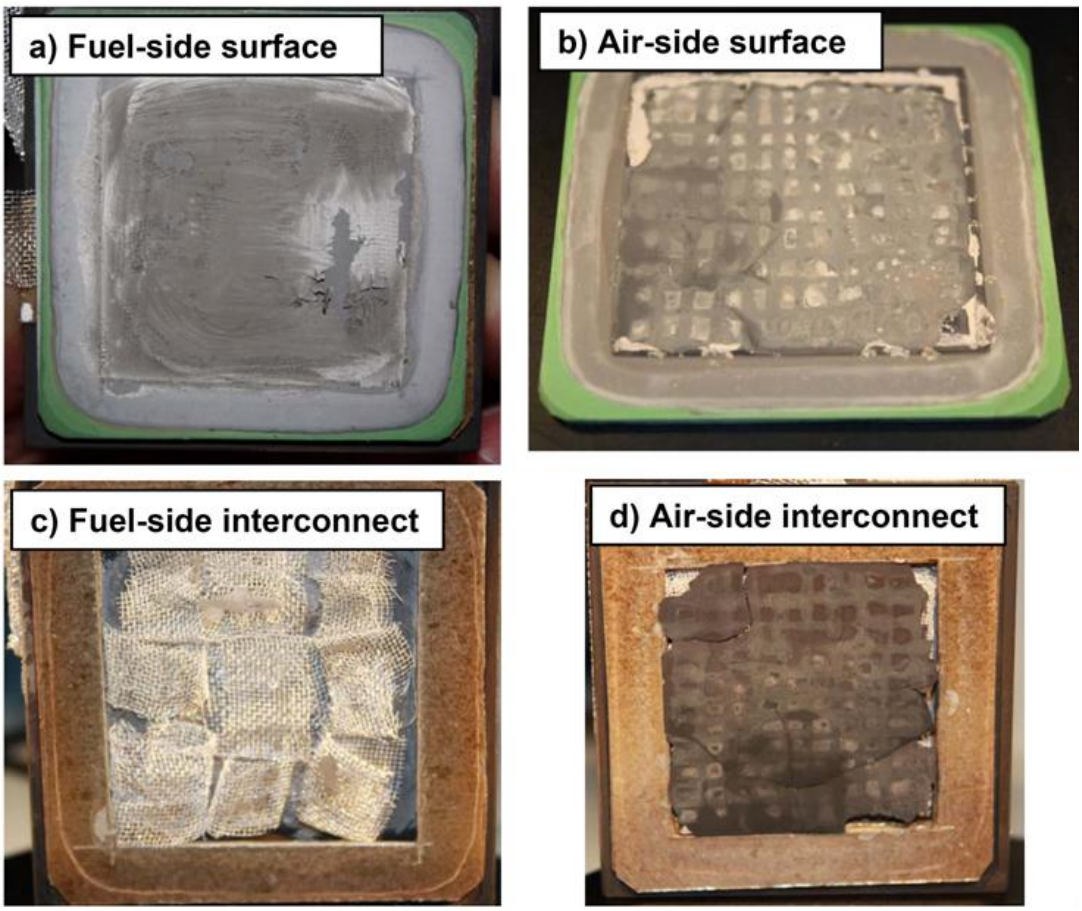

Figure 6: Photographs of VPS Cell 5 after removal from the test fixture.

shown in Figure 6. Upon removal of the interconnects, the air-side electrode delaminated from the electrolyte, and was found to be well adhered to the silver current collectors. The fuel-side electrode showed no irregular forms.

CSM is now in the process of evaluating the source and / or cause of the delamination. We have conducted X-Ray Diffraction (XRD) analysis on an air-side electrode prior to testing (as received from VPS), and compared it with the XRD signal obtained from the surface of the delaminated air-side electrode of Cell 5. This analysis is used to detect material phases in the electrodes; comparison of XRD signals can highlight the existence of phases or materials that are unique to each electrode.

As we are comparing the XRD signal from the exposed electrode surface of the untested cell with a signal from a material that was initially located at the electrode-electrolyte interface (triple-phase boundary region) for VPS Cell 5, we expect to see some differences in composition. The comparison is shown in Figure 7; noticeable differences include the (blue) VPS Cell 5 peaks at 30.7°, 35.6°, 51.0°, and 60.6°. These peaks are all attributed to ceria, which was applied to the electrolyte prior to deposition of the LSM cathode during cell fabrication at VPS. Of greater concern is the existence of the peak at 28.1° for the long-term tested cell; this peak is not found in the (pink) signal from the untested cell. XRD-library analysis indicates that this peak may be due to a lanthanum zirconate, or a yttria-ceria oxide phase. Previous researchers have detected the formation of the lanthanum zirconates at the electrode / electrolyte interface, and have attributed this resistive phase to cell degradation. Further analysis at CSM is ongoing to investigate this further, including SEM imaging. Additionally, VPS Cell 6 has been packaged into the test stand, and is being prepared for electrochemical testing during the time of writing of this report.

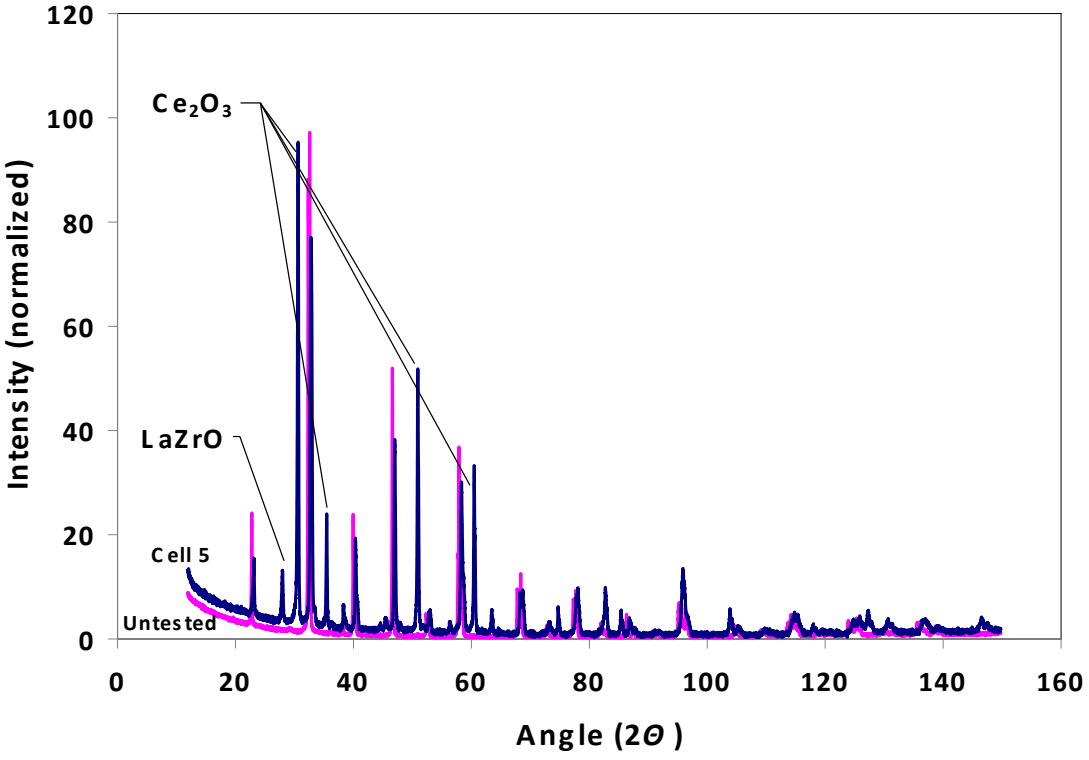

Figure 7: Comparison of XRD signals from air-side electrode of the as-received and long-term tested cells

APPENDIX B

Shows the XRD pattern report on lanthanum zirconates on the form of $La_2Zr_2O_7$. Taken from the XRD database in the XRD lab.

APPENDIX C

Short description of the test stand and its components.

APPENDIX D

Figure 4.14 - SEM images of reference cell: a) profile, b) oxygen electrode and c) hydrogen electrode

a)

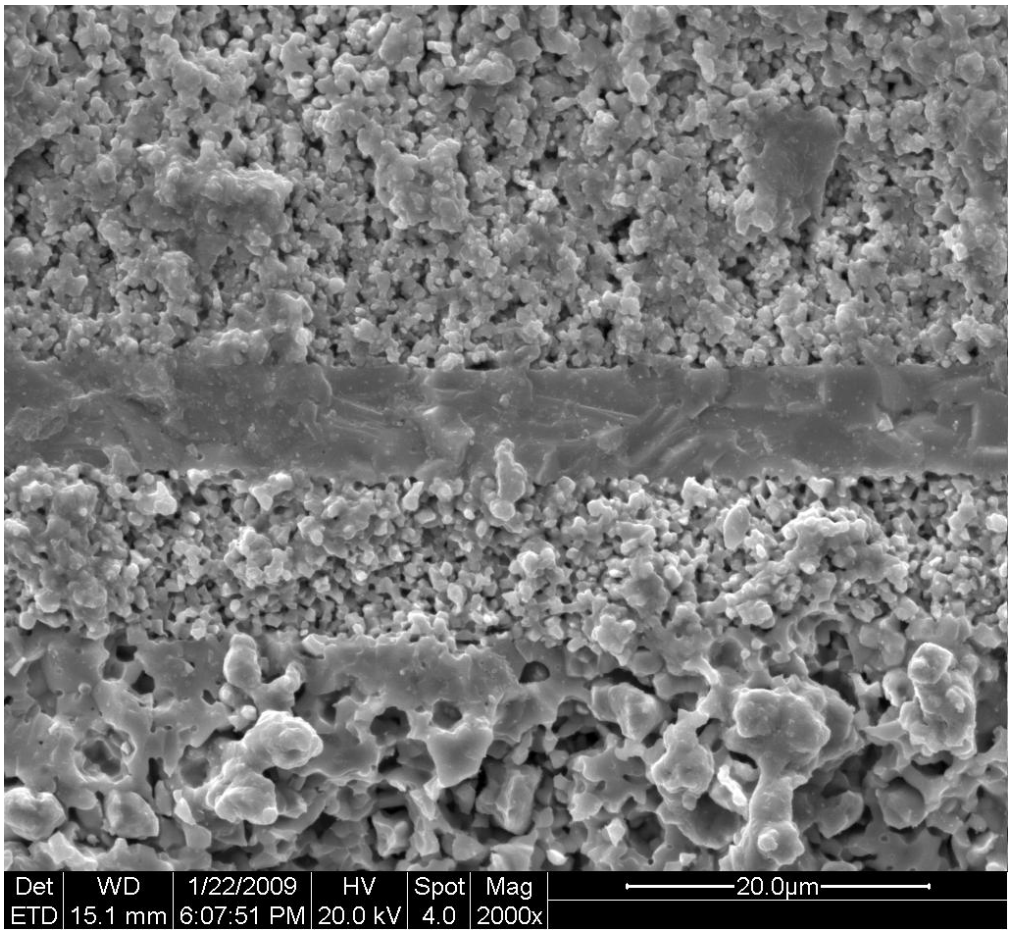

b)

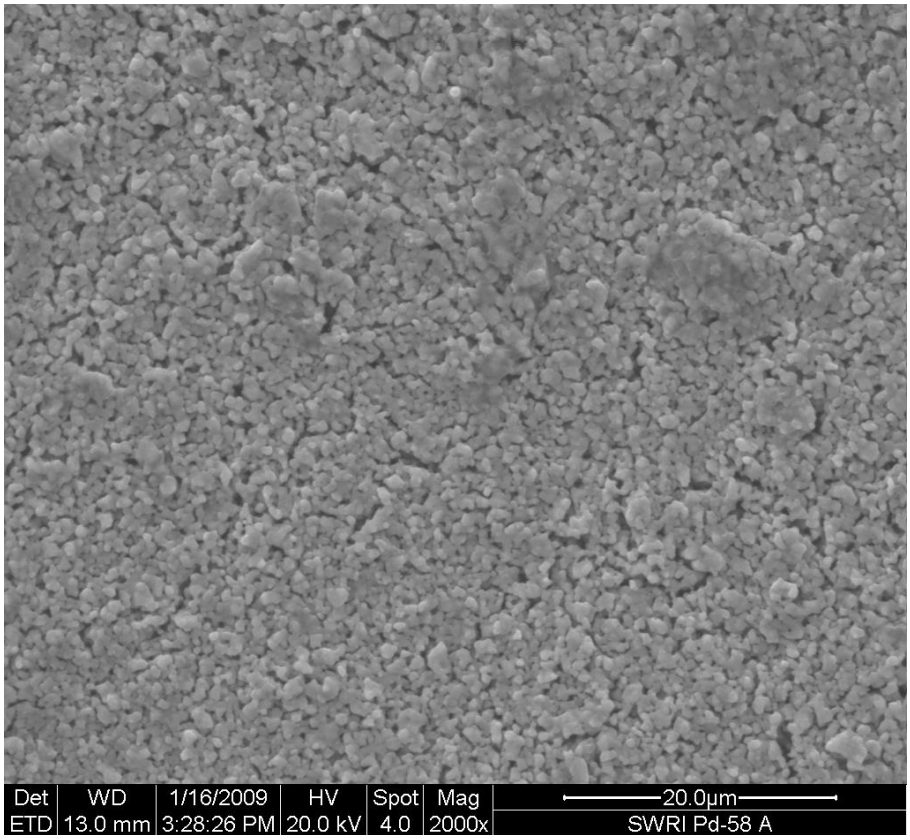
Det WD 1/16/2009 HV Spot Mag 20.0µm
ETD 13.0 mm 3:28:26 PM 20.0 kV 4.0 2000x SWRI Pd-58 A

c)

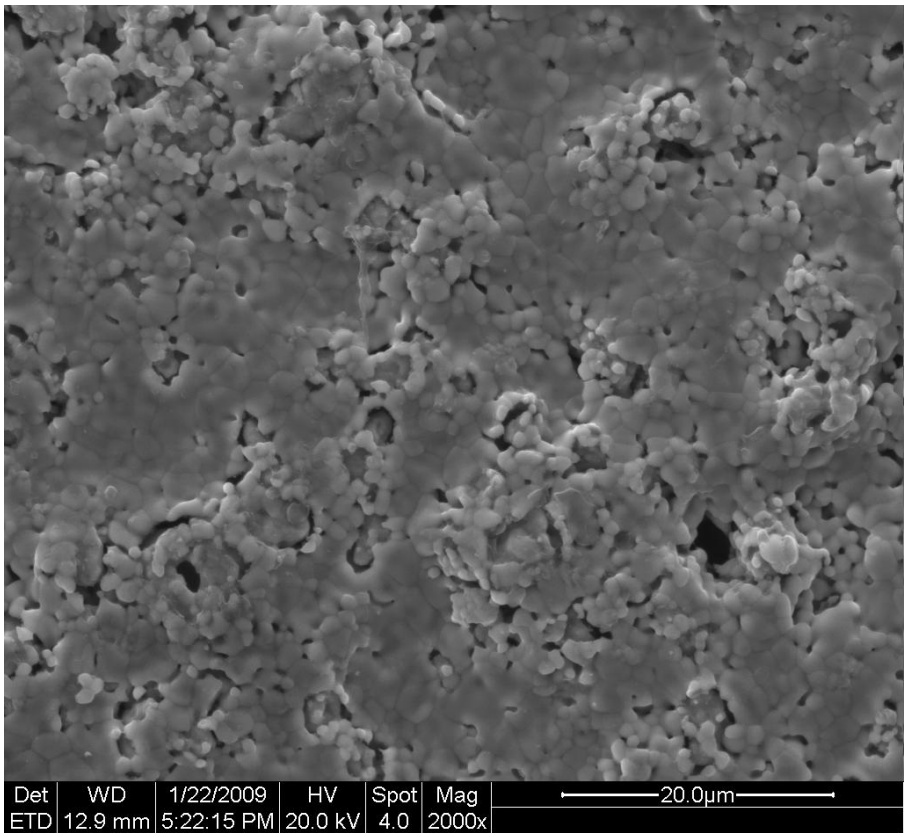
Det WD 1/22/2009 HV Spot Mag 20.0µm
ETD 12.9 mm 5:22:15 PM 20.0 kV 4.0 2000x

Figure 4.15 - SEM images of old cell: a) profile, b) oxygen electrode and c) hydrogen electrode

a)

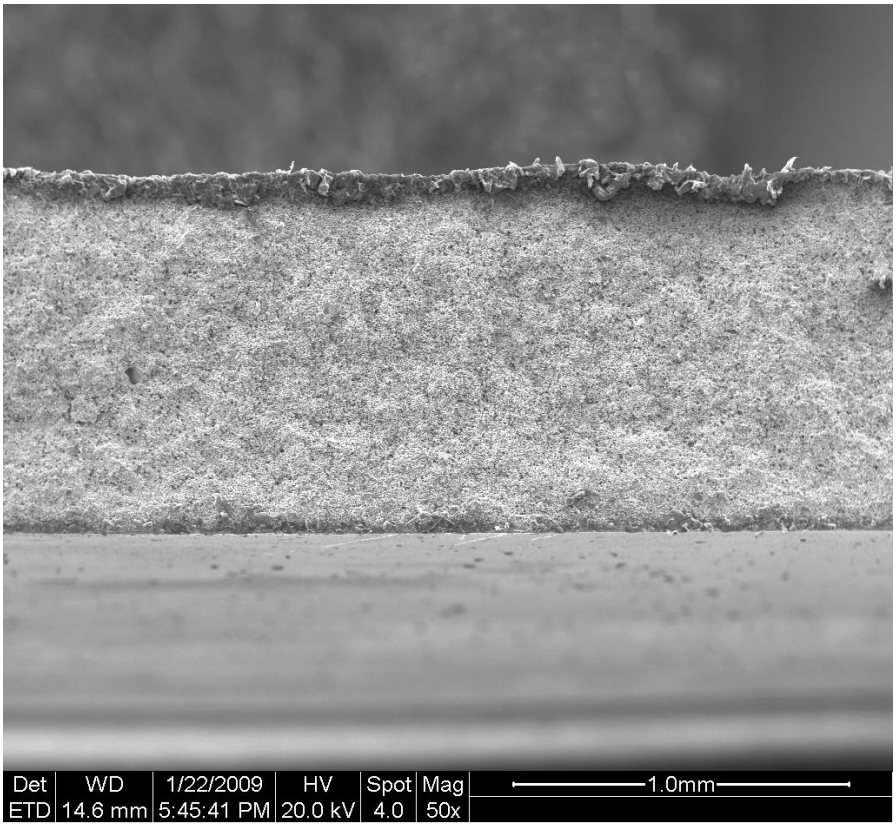

b)

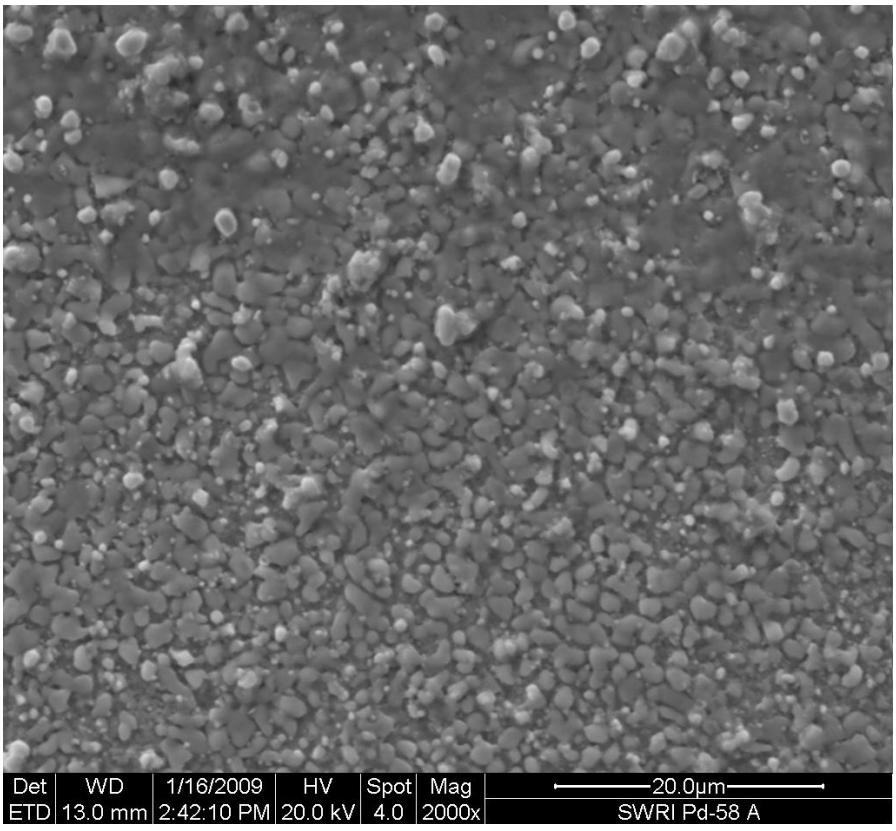

c)

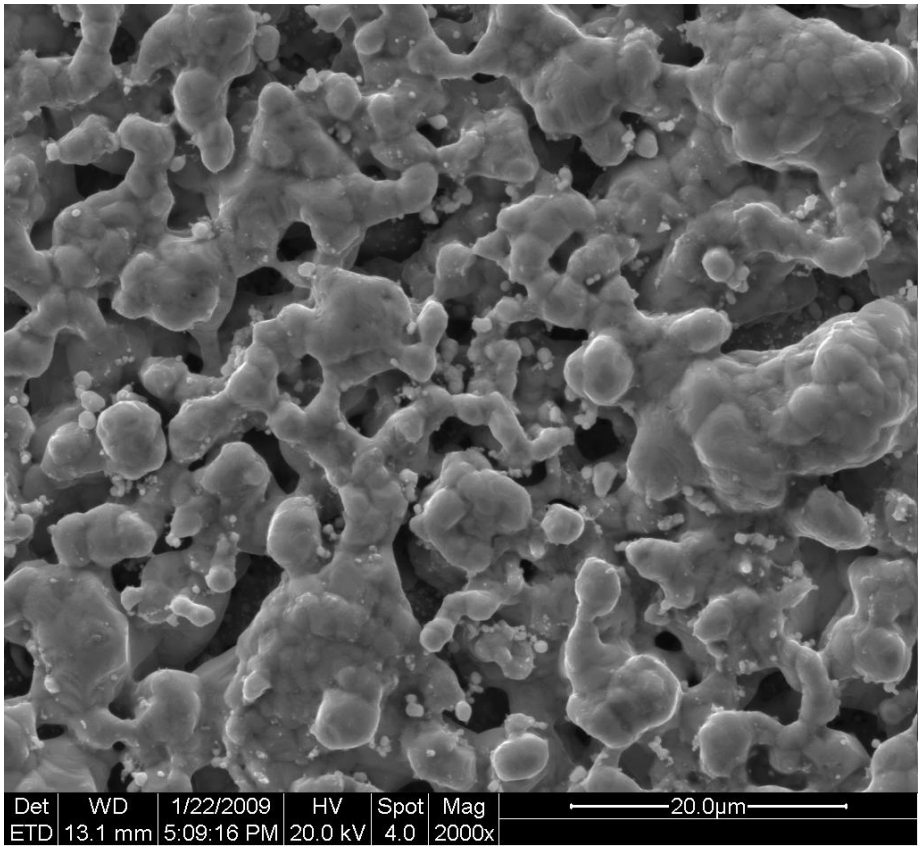

Figure 4.16 - SEM images of the two zones present in the delaminated electrode

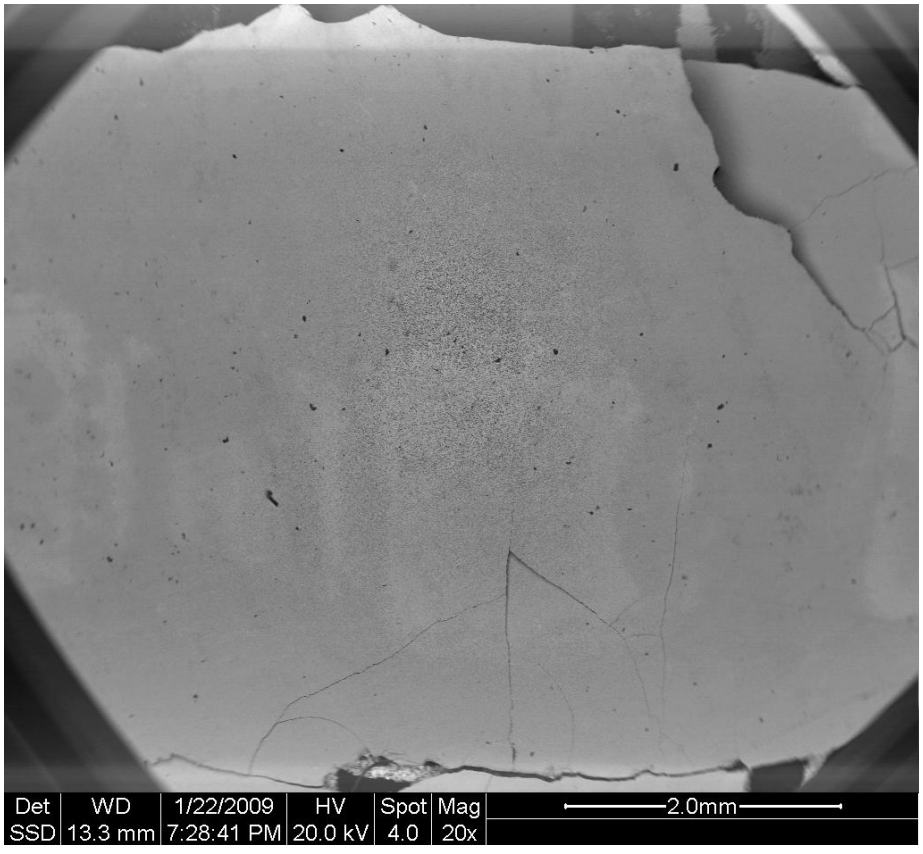

b)

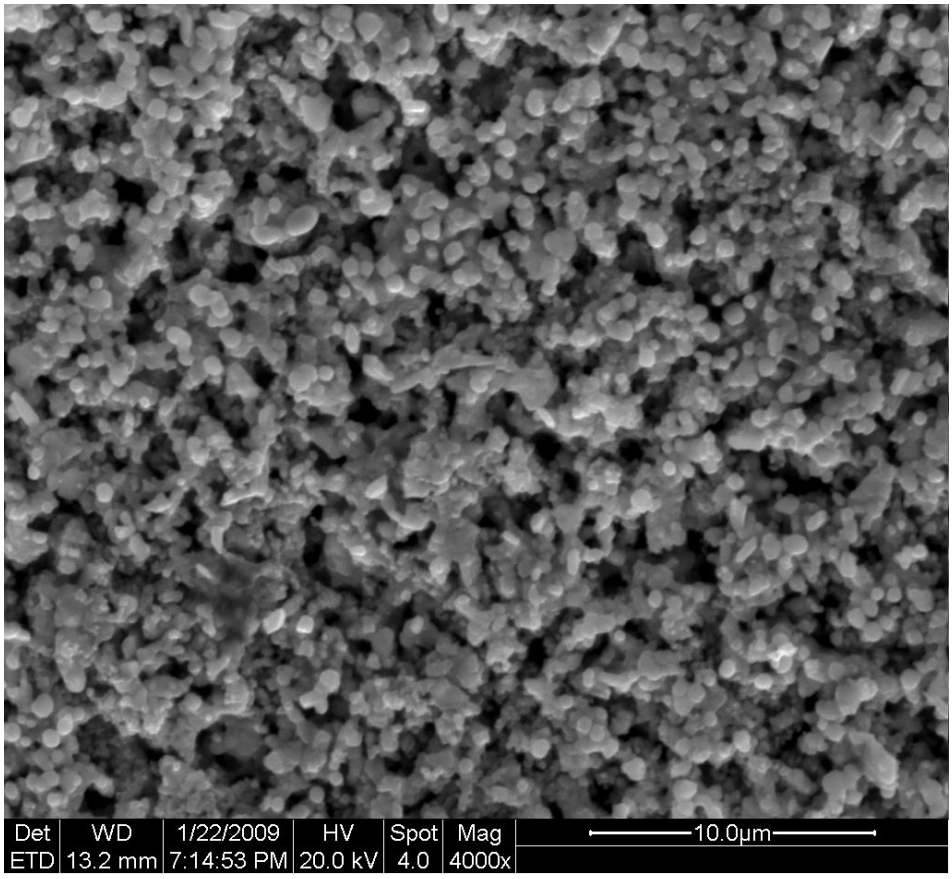
Det WD 1/22/2009 HV Spot Mag
ETD 13.2 mm 7:14:53 PM 20.0 kV 4.0 4000x
10.0µm

c)

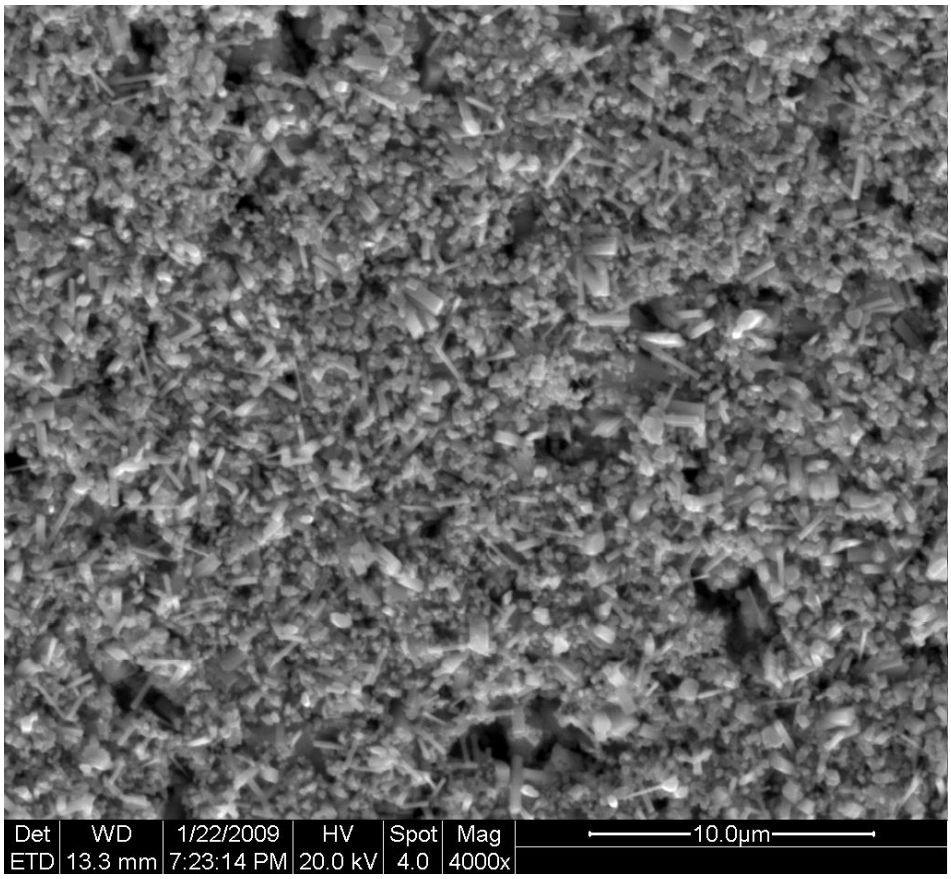
Det WD 1/22/2009 HV Spot Mag
ETD 13.3 mm 7:23:14 PM 20.0 kV 4.0 4000x
10.0µm

Figure 4.17 - SEM images of VPS cell 3: profile, oxygen electrode and hydrogen electrode

a)

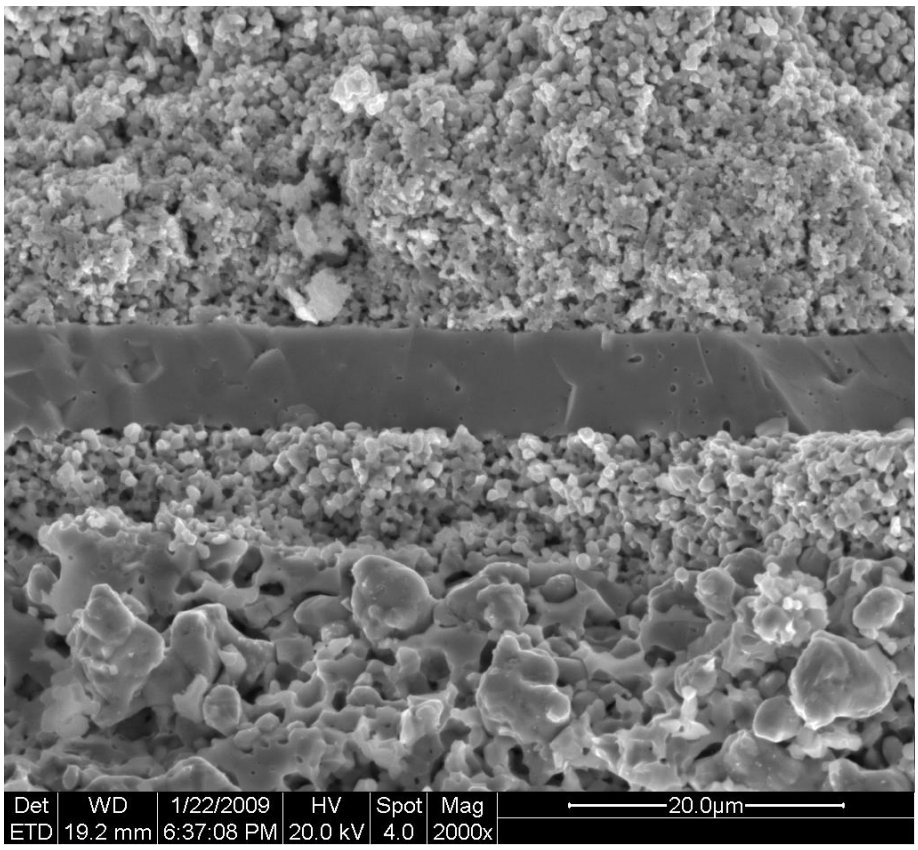

b)

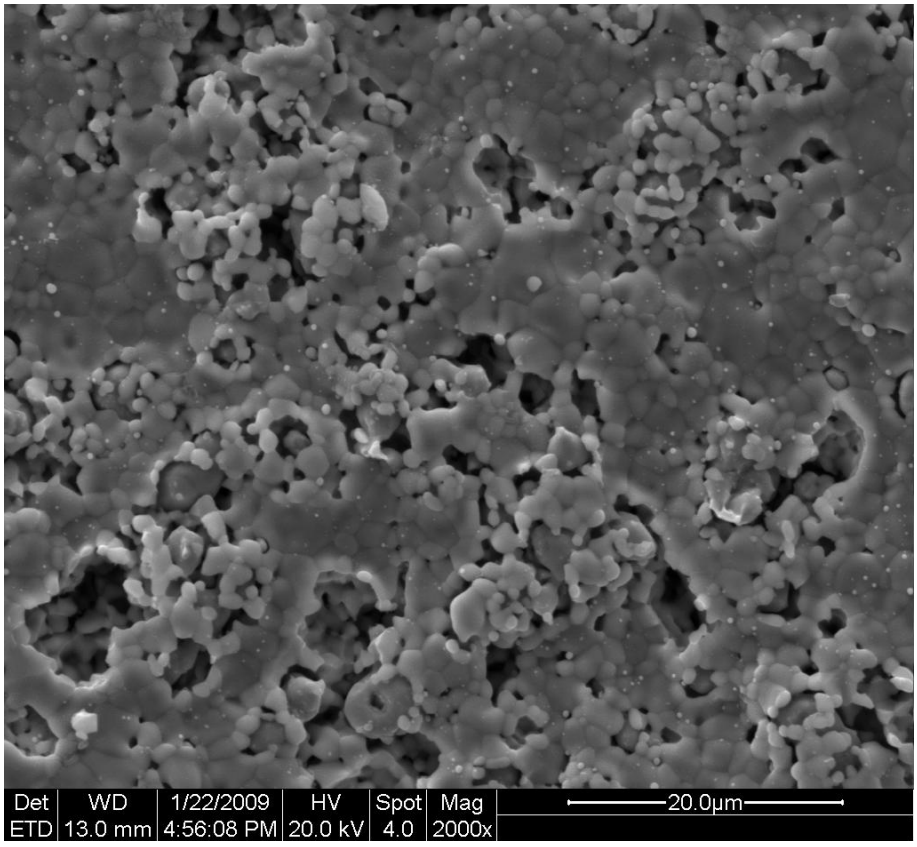

c)

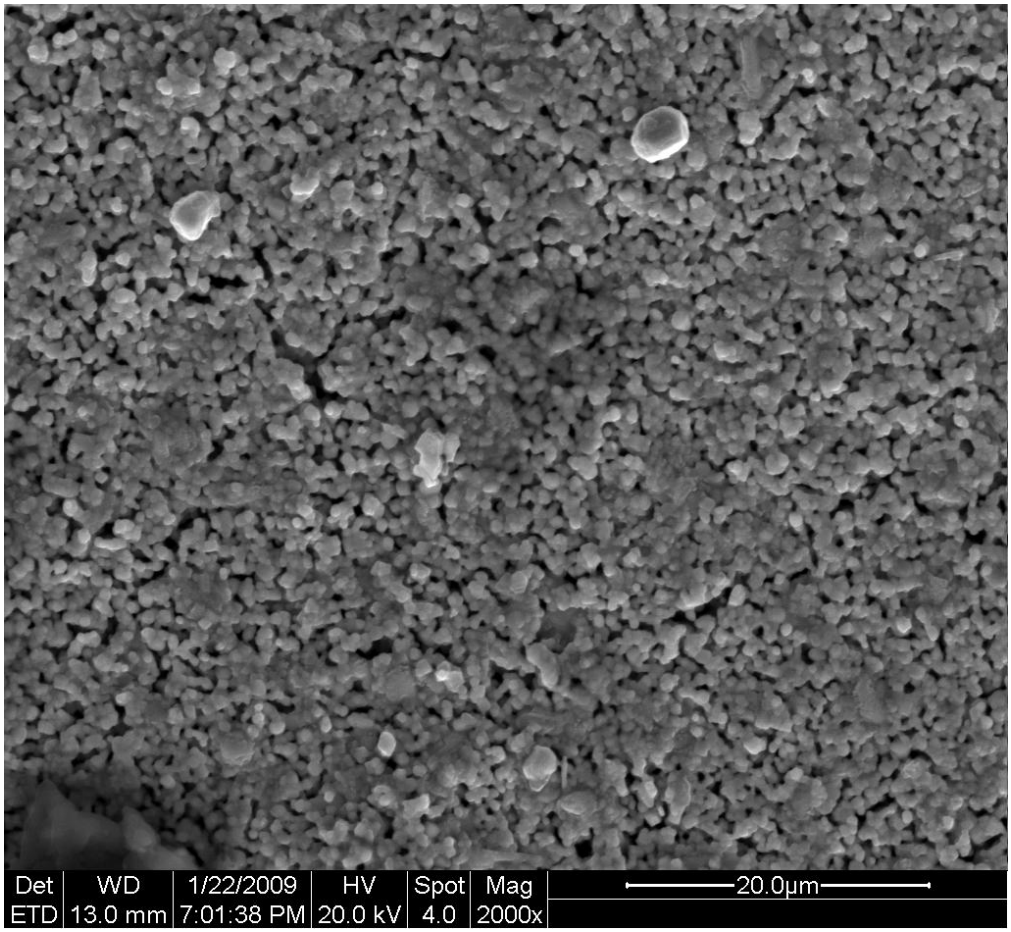
Det
ETD
WD
13.0 mm
1/22/2009
7:01:38 PM
HV
20.0 kV
Spot
4.0
Mag
2000x
20.0µm

Table of Contents

Description **Page Number**

1 Operating procedure

1.1 Cell Stack

After the cell stack has been set up with electric conductors and sealing devices, install the stack into the oven. In order to ensure a proper seal use the jack and spring system to apply pressure to the stack. Pack insulation around the gas inlet/outlet lines and secure silver wires to the four point probe connections; ensure they do not create a short-circuit.

1.2 Furnace

Once the stack and all of its connections are complete the furnace needs to be brought to temperature. Using the furnace temperature controller set the desired temperature and allow time for it to reach that temperature.

1.3 LABVIEW

After the furnace is at the desired temperature the LABVIEW then needs to be set up. Follow the on-screen instructions for the desired test environment. In order for the mass flow controllers to operate the switch above the rotameter corresponding to the test gas needs to be flipped to the upward “ON” position.

1.3.1 LABVIEW Tips

- The variable load can be controlled for either a constant current or constant voltage.
- LABVIEW will stop if the load temperature is not within safe operating range, (<150 Degrees Centigrade).
- If the test is for a prolonged period of time the refresh rate should be set lower because Microsoft Excel can only hold 32,000 data points.
- Unless the test is time specific the “Indefinite” button should be on. If a specific time is chosen the program will quit running after that specified amount of time.
- To run the VI while the furnace is warming up set “Desired V, I” to -1. This will create an open circuit on the cell until you are ready to apply a load.
- Once you are ready to apply a load set “Desired V, I” to your desired value. The VI will take a few minutes to achieve your desired value.
- The forming gas MFC is also the Ar MFC.

1.4 Test Completion

1.4.1 Ending Test

- Allow time for the furnace to cool down before opening.
- Click Stop Button in VI. **Do not** use stop button in the tool bar!
- Navigate to the chosen file path to analyze the data.

1.4.2 LabVIEW Output

- LabVIEW will output the following data in the following order
    - Elapsed Time
        - LabVIEW outputs time in seconds. However, in order to have Excel auto format the time you need to divide this number by 86,400. Then you can have Excel format it as 00:00:00.
    - Voltage across the Cell in Volts
    - Current produced by the cell in Amps
    - Power produced by the cell in Watts
    - Temperature of the load in degrees Celsius
    - Control Voltage to load
    - Flow rate of Ar in SLM
    - Flow rate of H_2 in SLM
    - Flow rate of CH_4 in SLM
    - Flow rate of Air in SLM

2 Layout of the Test Stand

2.1 Circuit Connections

2.1.1 DAQ Input

Channel	Signal Use	Wire Color
3	H_2	Blue
4	CH_4	Green
2	Ar	Yellow
15	Air	Light Brown
1	I^+ (Differential)	Belden Cable
9	I^- (Differential)	Belden Cable
0	V^+ (Differential)	Belden Cable
8	V^- (Differential)	Belden Cable
11	Load Temperature	Dark Brown
AISN	0 Volts	White
14	V_{in} from load control	White (from AO0)

2.1.2 DAQ Output

Channel	Signal Use	Wire Color
3	H_2	Grey
4	CH_4	Pink
2	Ar	Red
8	Air	Purple
0	V_{out} to load control	Belden Cable
+5V	5V terminal	Orange

2.1.3 Terminal Block Connections

- 12V Strip
  - All solenoid valves
  - Watts up meter (inline current/voltage meter)
- +15V Strip
  - All MFC Pin 11 connections
- -15V Strip
  - All MFC Pin 9 connections
- 5V Reference
  - All MFC Pin 15 connections
  - Load temperature sensor

2.1.4 MFC Connector Wiring

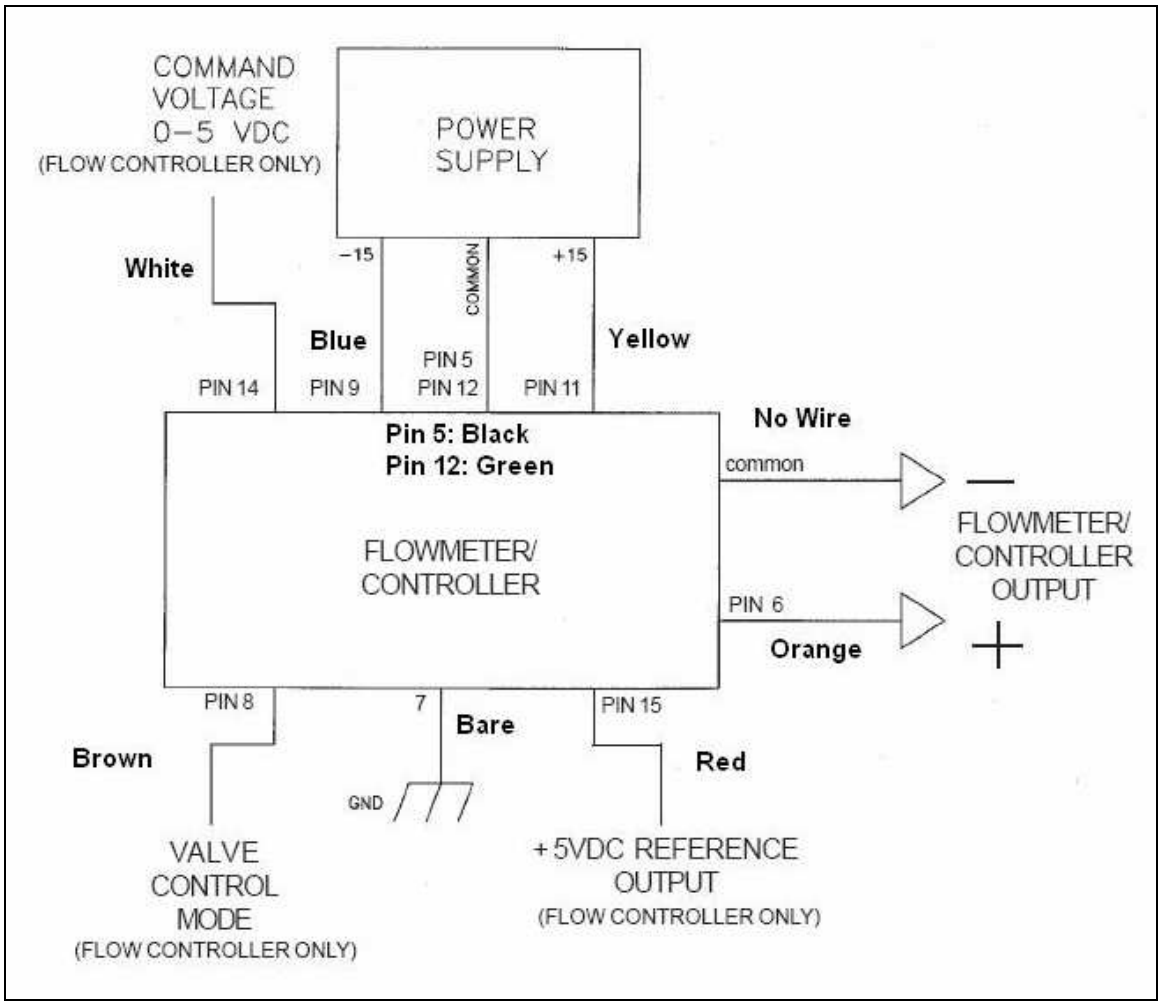

Figure 1: MFC Connections, image provided by Teledyne-Hastings.

2.1.5 Overall Stand Circuit Diagram

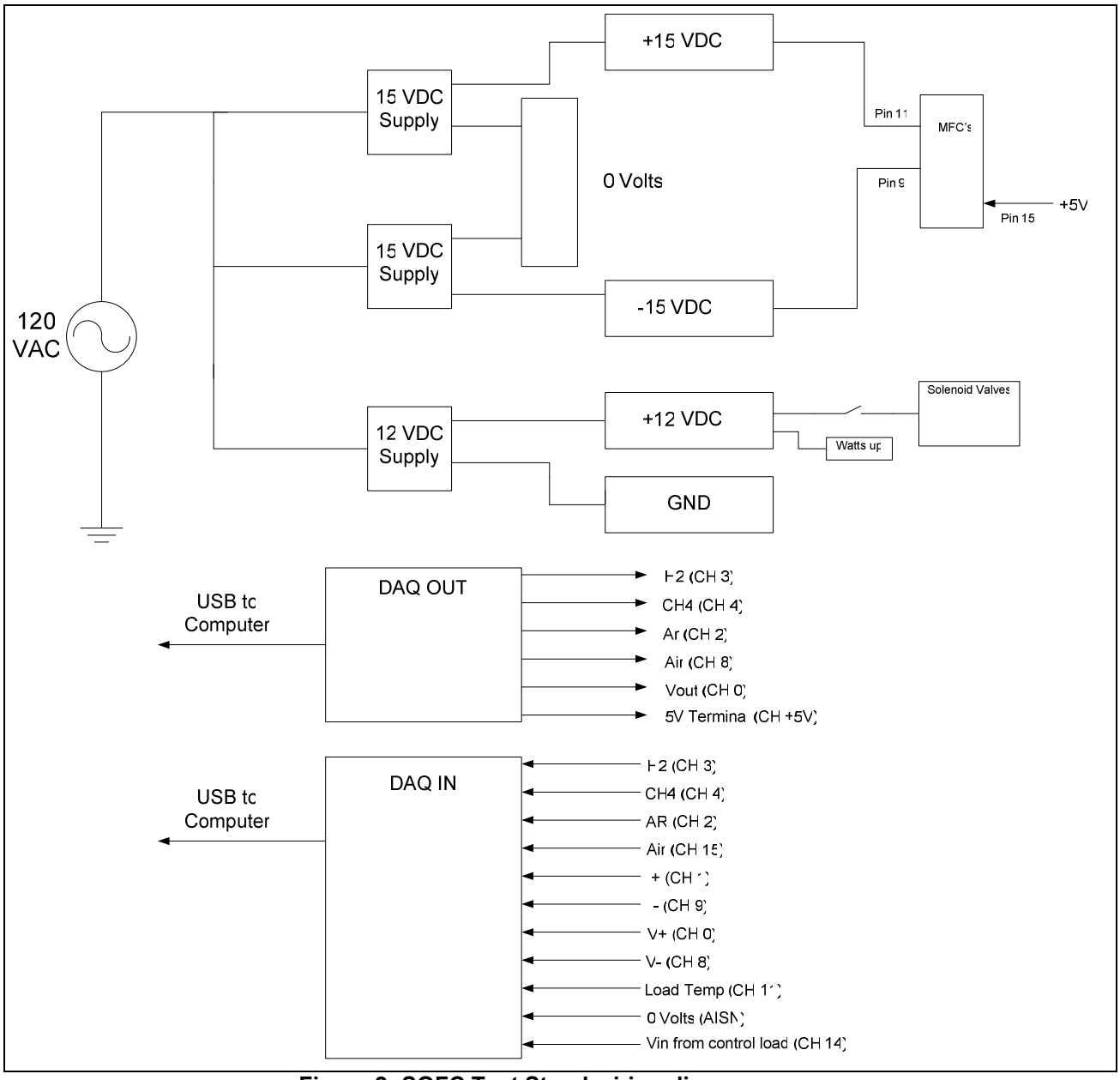

Figure 2: SOFC Test Stand wiring diagram

2.1.6 *Circuit Schematic for Load*

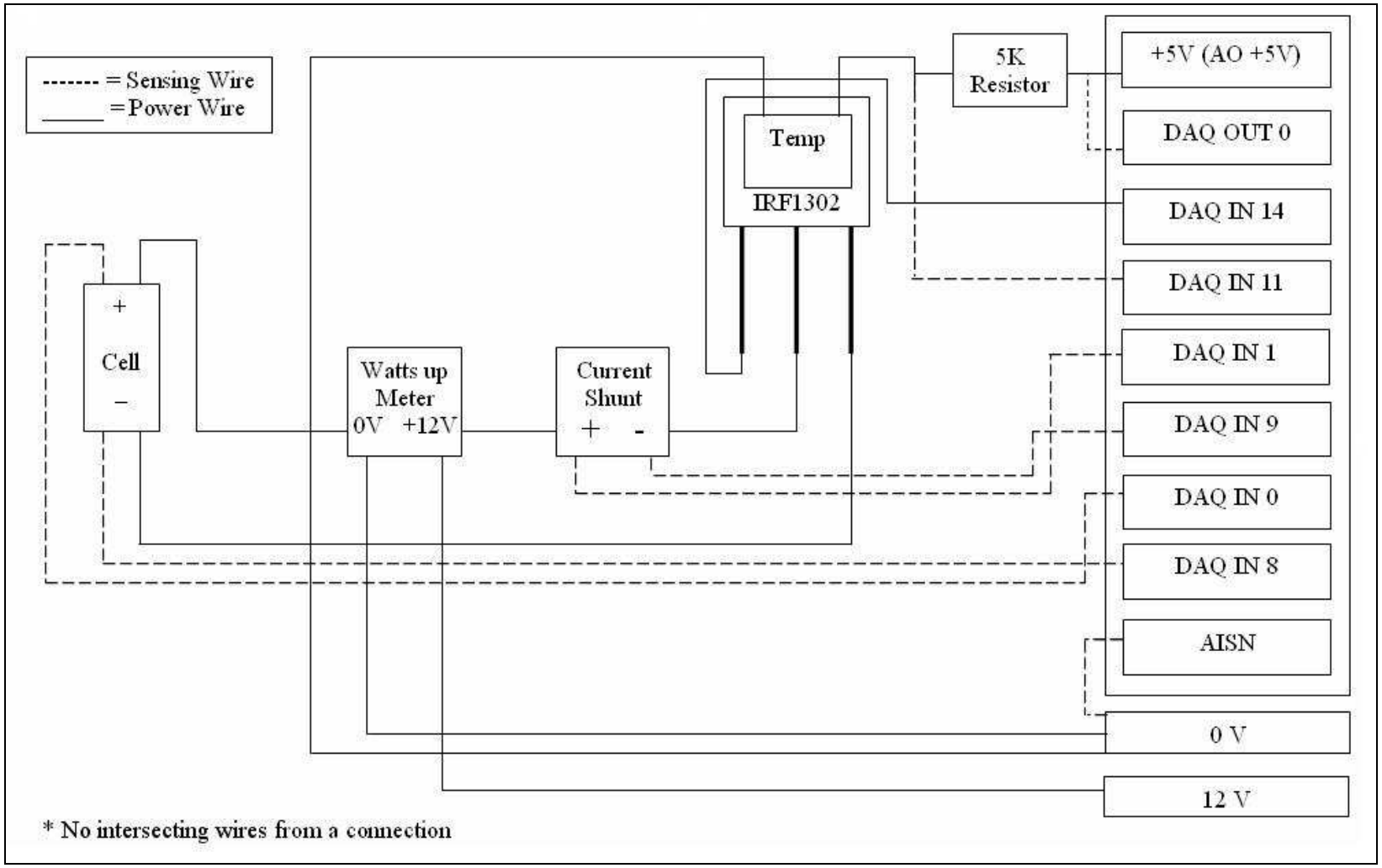

Figure 3: Circuit Schematic for Load

2.2 Fluid Flow Diagram

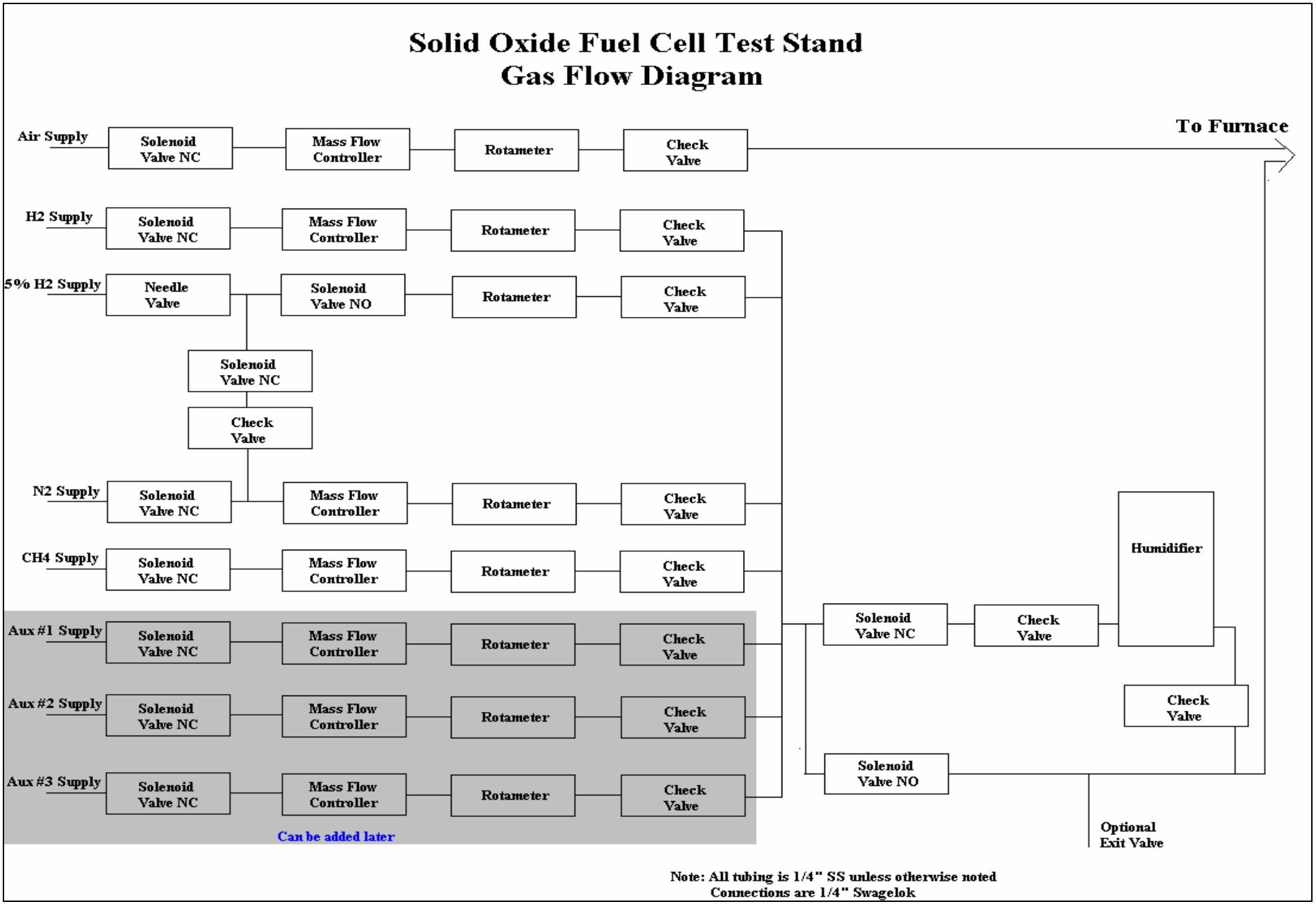

3 Individual Test Stand Components

The following is a list of all of the components and where applicable their part/model numbers. The parts that have individual manufacturer manuals are included either on the CD-ROM or as stand alone documents.

- Asco Normally Open solenoid valves
  - Catalog # 8262-G138-12/DC
- Asco Normally Closed solenoid valve
  - Catalog # 8262-G007-12/DC
- Teledyne Hastings mass flow controllers
  - Model # HFC-202
- ABB rotameters
  - Model # 10A6132AB1B
- Applied Test Systems furnace
  - Series 3210, Serial # 07-1849
- Applied Test Systems furnace controller
  - Series 2404 (Barber-Colman/Eurotherm)
- Swagelok check valves
  - SS-4C1-1/3
- Swagelok needle valve
  - SS-14DKS4
- Humidifier
  - Supplied by CFCC
- Mean Well 15 VDC power supply
  - Model # PSU40A-4
- Mean Well 12 VDC power supply
  - S-320-12
- National Instruments input DAQ
  - NI-USB-6210
- Measurement Computing output DAQ
  - USB-3105
- Toggle switches
- Terminal blocks
- Belkin power strip
- Dell XPS computer
- Watts-up meter

4 Machined Components

The following list of components was machined specifically for this test stand and can be replaced. The drawings for each part can be found at the end of this manual and also on the CD-ROM.

- Ceramic Compression Plate
- Gas Manifold
- Spring Enclosure Cylinder (Spring Support Pt. 1)
- Spring Mount for Ceramic Rod (Spring Support Pt. 2)
- Jack Mount for Ceramic Rod (Spring Support Pt. 3)